TRENDS IN SCIENCES 2025; 22(11): 10929
https://doi.org/10.48048/tis.2025.10929 RESEARCH ARTICLE

Optimized Microencapsulation of *Citrus aurantiifolia* Peel Extract for Breast Cancer Therapy: *In Silico*-Supported Approach

Angelica Kurnia Herjandi, Jamaludin Al-Anshori and Euis Julaeha*

Department of Chemistry, Faculty of Mathematics and Natural Sciences, Universitas Padjadjaran, Jatinangor 45363, Indonesia

(*Corresponding author's email: euis.julaeha@unpad.ac.id)

Received: 12 June 2025, Revised: 13 June 2025, Accepted: 18 June 2025, Published: 10 August 2025

Abstract

Breast cancer is the most prevalent cancer in Indonesia and is primarily treated by surgery or chemotherapy, often accompanied by adjuvant therapy. *Citrus aurantiifolia* peel extract exhibits potential as a natural anti-cancer compound. *In silico* screening identified 16 out of 95 candidate compound–protein interactions that demonstrated strong binding to key breast cancer-related targets (3ERT, 3PY0, 8I0M, 7PG6, and 1KV1), suggesting therapeutic relevance. Due to the extract's environmental sensitivity, encapsulation is necessary to preserve its bioactivity. This study employed complex coacervation using a gelatin–gum arabic system crosslinked with glutaraldehyde, with formulation parameters optimized to improve encapsulation performance. The extract yield was 11.40%, and the optimal formulation ratios were 3.74:4 (extract/matrix), 0.066:4 (crosslinker/matrix), and 2:2 (gelatin/gum arabic). The resulting microcapsules achieved a yield of 54.21 ± 4.76%, an extract content of 3.67 ± 0.24%, and an encapsulation efficiency of 99.65 ± 0.09%, with spherical morphology and an average size of 1.249 ± 0.710 µm. Release studies followed Higuchi kinetics, indicating a controlled diffusion profile. These findings support the potential of *C. aurantiifolia* peel extract as a stable, encapsulated anti-cancer candidate for future therapeutic applications.

Keywords: *Citrus aurantiifolia*, *In silico*, Optimization, Microencapsulation, Complex coacervation, Breast cancer, Adjuvant therapy

Introduction

One category of dangerous diseases that cause human death worldwide is cancer [1]. According to data from the Global Cancer Observatory (GCO) in 2020, breast cancer ranks as the leading cause of death in Indonesia, accounting for 59.1% of deaths, or approximately 234,511 individuals, and growing at a rate of 16.6%, or approximately 396,914, out of the total recorded population of 273,523,621. Generally, the main procedure for treating cancer is surgery or chemotherapy, followed by adjuvant therapy.

Adjuvant therapy, an advanced therapy, aims to boost the body's immunity for disease-free survival (DFS) by managing micrometastases that could potentially spread throughout the body [2]. The goal of adjuvant therapy is to kill residual cancer cells found after the main procedure and prevent them from growing, as well as spreading to other areas in the body.

In vitro tests were done by Kenyori *et al.* [3] and Gomathi *et al.* [4] using human breast adenocarcinoma, which is made up of differentiated breast glandular epithelium. Hormonal therapy requires the antagonistic properties of active compounds to inhibit the action of estrogen hormones in cancer cell proliferation. These useful chemicals are found in many plants, like the lime (*Citrus aurantiifolia*): flavonoids, coumarins, fatty acids, and limonoids [5]. One of the flavonoid compounds found in *C. aurantiifolia*'s peel is quercetin, which can help fight cancer by stopping cell growth, stopping growth factors, and protecting cells from damage. Therefore, this study aims to harness the

anticancer activity of *C. aurantiifolia* extract. We use the extract form of *C. aurantiifolia* peel to determine its effectiveness as a therapeutic or pharmacological agent.

According to Marcillo-Parra *et al.* [6], the extract of plant material often contains active compounds that are unstable to environmental conditions such as oxygen, humidity, or unfavorable storage conditions. Therefore, we need a technique called microencapsulation to maintain the quality of active compounds in plant material extracts [5]. Microcapsules consist of encapsulated material, commonly referred to as core material or internal phase. Meanwhile, we refer to the encapsulating material as the matrix, coating, shell, or external phase. Many methods, including physical, chemical, and physico-chemical ones, are available for the manufacture of microcapsules.

Complex coacervation is the most widely used method because it does not require high costs, does not use solvents, and is suitable for application to hydrophobic compounds [7]. This method uses one or more charged coating polymers that combine proteins and polymers. Gelatin and gum arabic polymer were used as a matrix because they work well together because they dissolve easily in water, stay stable in colloidal form, and let active ingredients release slowly [8]. However, the mechanical strength of these matrices is low, and they dissolve relatively quickly, limiting their practical application. By adding crosslinking agents, we can overcome these shortcomings and improve their chemical stability and mechanical properties. People commonly use crosslinkers with aldehyde groups, like glutaraldehyde, to enhance strength and durability because of their long-term stability [9].

Previous studies have reported the bioactivities of *C. aurantiifolia* as insecticides, larvicides, anti-mosquitoes, antioxidants, anticancer, antimicrobial, antiseptic, antiviral, antifungal, astringent, anticholesterol, diuretic, appetite stimulant, constipation medicine, anti-inflammatory, and analgesic in both extracts and essential oils [10]. According to *in silico* tests, the quercetin compounds in *C. aurantiifolia* peel have a lower affinity energy than the native ligand (DRO) protein 2W3L in MCF-7 breast cancer cells. This indicates that quercetin can bind more strongly to the receptor than the original ligand [3]. This is supported by the results of the *in vitro* test of the ethanol extract of *C. aurantiifolia*, the compounds 5-geraniloxy-7-methoxycoumarin, 5-geraniloxipsoralen, and 8-geraniloxipsoralen, which have IC_{50} of 72.810, 246.085, 147.514, and 429.33 µg/mL, respectively [11]. Therefore, we can assert that the extract of *C. aurantiifolia* exhibits superior anticancer activity compared to its pure isolate. Furthermore, reports have documented the activity of *C. aurantiifolia* in various compositions, coatings, and crosslinkers for diverse purposes.

A previous study by the authors developed alginate–gelatin hydrogel microbeads to encapsulate *C. aurantiifolia* peel extract for antibacterial wound dressing applications [12]. Expanding on this foundation, the present study adopts a complex coacervation method using a gelatin–gum arabic system to enhance encapsulation efficiency and achieve a more controlled release profile. Additionally, *in silico* analysis was performed to evaluate the interactions between bioactive compounds in the extract and selected breast cancer–related protein targets. This computational approach was employed to support the extract's therapeutic relevance in oncology, rather than to guide formulation development. The combination of improved encapsulation and molecular docking analysis highlights the novelty and potential impact of this work in the context of breast cancer therapy.

To date, existing literature has no research on breast cancer target proteins and the optimized coating proportions of *C. aurantiifolia* microencapsulation. In this research, the *in silico* interaction of *C. aurantiifolia* extract constituents with target proteins of breast cancer is explored while optimizing inter-coating, crosslinker, and extract-to-coating ratios to create optimal *C. aurantiifolia* peel extract microcapsules that retain anticancer properties.

We employed a complex coacervation method, combining gelatin and gum arabic polymers as the coating material, *C. aurantiifolia* peel extract as the encapsulated material, and glutaraldehyde as the crosslinker. Variations in the ratio of encapsulated *C. aurantiifolia* peel extract were 0.55, 1.64, 2.70, 3.74 and 4.76% to the coating. We varied the composition of the glutaraldehyde as a crosslinker to 0.052, 0.059, 0.066, 0.073, and 0.080%. We also varied the composition of the coating (gum arabic:gelatin) to 1, 1.5, 2, 2.5, and 3%.

We replicated each variation of extract, crosslinker, and coating 3 times using a triplo method. To characterize the microcapsules, we assessed their yield, encapsulation efficiency (%EE), extract content (%EC), functional group (FTIR), morphology (SEM), particle size and distribution (PSA), and thermal stability (TGA). We also observed the release rate of *C. aurantiifolia* peel extract from the microcapsules to ascertain the amount and mechanism of extract release.

Materials and methods

In this section, we meticulously outline the materials and methodologies employed in our study. The selection of materials was based on their relevance to the research objectives, ensuring that each component contributed effectively to the overall investigation. Furthermore, we employed rigorous methodological approaches, including both qualitative and quantitative analyses, to ensure the reliability and validity of our findings.

Materials

We will provide detailed descriptions of experimental procedures, data collection techniques, and analytical frameworks to ensure reproducibility and transparency in our research. Caringin Village, located in the Bandung Kulon District of Bandung City, provided the fruit peel for the research. This study by Pandiangan *et al.* [13] used a Buchi rotary evaporator model R-200, a Perkin-Elmer Lambda 35 UV-Vis spectrophotometer, a JEOL JSM-6510 scanning electron microscope, and a Beckman Coulter LS 13 320 particle size analyzer. These were the most important tools used in the study. These tools facilitated precise measurements and analyses, ensuring the reliability and accuracy of the findings.

The modified literature Pandiangan *et al.* [13], Huang *et al.* [14] provided the study's materials. These materials included distilled water as a solvent, ethanol redistilled for the maceration extraction process, and UV-Vis for characterization. We obtained the UV-Vis from the Natural Product Chemistry and Synthesis Laboratory, Universitas Padjadjaran. We obtained the food-grade gum arabic and gelatin from Kimia Market and used glutaraldehyde as a crosslinker in the microencapsulation process.

In-silico analysis

In silico studies are essential as they provide crucial insights into molecular interactions between bioactive compounds and carrier materials before physical experimentation, enabling researchers to predict compatibility, stability, and release kinetics while optimizing formulation parameters. Additionally, molecular docking simulations reveal binding affinities between extract compounds and protein of breast cancer cell targets, offering a rational basis for designing encapsulation systems that enhance therapeutic efficacy while reducing development costs and experimental timeframes.

MCF-7 is an estrogen receptor-positive breast cancer cell line, making it highly relevant for research focused on hormone-based therapies. MCF-7 is also used to study mechanisms of resistance to therapy, including resistance to CDK-2 inhibitors and hormonal therapy [15].

Protein structure 8I0M, as an MT1-MMP crystal complex, has shown promising effects in modulating key signal pathways of the epithelial-mesenchymal transition (EMT), a process that plays a role in cancer metastasis [16]. MT1-MMP, specifically, has a pertinent role in migration and viability induction in MCF-7 cells. This points to its therapeutic application, particularly in addressing invasive breast cancer behavior. Furthermore, insights into cell reprogramming and resistance mechanisms to proteins like MT1-MMP can be utilized to enhance the efficacy of drugs traditionally used in the therapy of breast cancer, such as doxorubicin [17].

In addition, protein 7PG6 plays a structural function in pro-apoptotic pathways, which can be therapeutically targeted in MCF-7 cells. It has been shown that targeting pro-apoptotic mechanisms enhances the cytotoxic effect of a range of clinically employed chemotherapeutic agents. The significance of this protein is also demonstrated by the fact that it interacts with tumor suppressor gene regulating pathways, whose inhibition leads to increased cancer cell viability [18,19].

Protein 1KV1 facilitates an understanding of how iron metabolism contributes to apoptosis and cell proliferation in breast cancer. The structure illustrates the connection between iron homeostasis and cancer cell

survival and reveals how disruption of these processes affects MCF-7 cells specifically [20,21].

The study is at an early stage. Among the key proteins that are researched in this work are cyclin-dependent kinase-2 (3PY0), whose key amino acids at the binding pocket are Asp145 and His84; estrogen receptor alpha (3ERT), whose key amino acids at the binding pocket are Asp351 and Glu353; 8I0M, whose key amino acids are Trp-636 and Tyr-647; 7PG6, whose key amino acids are Asp335, Tyr383, Gln384, Arg-307, and Thr-172 [22,23]; and 1KV1, whose key amino acids are unknown.

The estrogen receptor (3ERT) is a key target in breast cancer treatment, especially for estrogen-positive breast cancer. This receptor functions as a transcription factor that regulates the expression of genes involved in breast cancer cell growth and proliferation. When estrogen binds to 3ERT, there is activation of signaling pathways that promote cell proliferation. Therefore, inhibition of the interaction between estrogen and 3ERT can reduce cancer cell growth, making it an important target in breast cancer therapy [22,23].

On the other hand, CDK-2 is a key enzyme that regulates the transition from the G1 phase to the S phase in the cell cycle. Overexpression of CDK-2 has been identified in various cancers, including breast cancer, and contributes to resistance to therapy. CDK-2 inhibitors can stop cancer cell proliferation by inducing cell cycle arrest, making it an attractive target for cancer drug development [22].

These proteins are involved in key steps of cancer cell proliferation. The resulting insight, at a molecular level, would be valuable as to how such microcapsules could work while their effective therapies are being developed [24,25].

Protein preparation

The 3D X-ray crystal structure of ER-α (Protein Data Bank ID: 3ERT), CDK-2 (Protein Data Bank ID: 3PY0), CDK4 (Protein Data Bank ID: 8I0M), PI3K (Protein Data Bank ID: 7PG6), and MAPK (Protein Data Bank ID: 1KV1) was fetched from Protein Data Bank (PDB) (https://www.rscb.org, accessed on January 16th and February 19th, 2025) software package was used to prepare the protein. Furthermore, co-crystallized ligand was separated from the 3D structure of the protein and saved in PBD format, while the water molecules were removed from the ligand-free protein and saved in PDB format. The ligand and protein were processed using AutoDock tools (version 1.5.7), and saved in the pdbqt format.

Ligand preparation

The structures of 19 compounds reported in the literature [25-27] from *C. aurantiifolia* peel: murrayacarpin A; 2,4,4′,6′-tetrahydroxy benzophenone; evodin; bergaptol; crocetin; nobiletin; tangeretin; scoparone; sinensetin; and tetramethylscutellarein, 5-geranyloxy-7-methoxy coumarin; 5-geranyloxypsoralen; 8-geranyloxypsoralen; methyl isolimonate acetate; europetin; luteolin; limonin; 3`-hydroxygenkwanin; and myricetin as a reference drug (ligand) for breast cancer were drawn on 2D sketch program available in ChemDraw Professional v16.0 software package. All ligands were converted into the AutoDock tool (version 1.5.7) and then saved in pdbqt format.

Molecular docking studies

Molecular docking studies were performed using AutoDock Vina (version 1.2.0). First, the grid box parameter was set to a size of 40×40×40 with a 0.375 Å spacing, which covered co-crystallized ligand and the largest compound structure for docking. The docking poses generated by AutoDock Vina were separated using Vina Split, and the most preferred pose (with the lowest binding score) was superimposed onto co-crystallized ligand file. Subsequently, Root Mean Square Deviation (RMSD) was calculated using Biovia Discovery.

Molecular docking calculations were performed using Biovia Discovery at the binding site of 3ERT, 3PY0, 8I0M, 7PG6, and 1KV1 receptors with default parameters. No constraints were applied for all the docking studies. For each compound, multiple poses were attained after the molecular docking calculations containing the key residues involved in ligand binding.

In the 3ERT receptor, the key amino acids are Asp351 and Glu353; their presence allows the complexes of ligand and receptor to be in a stable form, which is quite necessary for the activation or inhibition of the receptor [28]. For example, good-interacting ligands to these parts induce a change in the shape of the receptor that enhances or reduces its biological activity, especially in the case of 3ERT-related breast cancer.

Whereas, in the case of the 3PY0 receptor, Asp145 and His84 are considered the essential amino acids. This participates in hydrogen bond development with the ligand and hence, helps maintain stability to the ligand-receptor complex, His84, on the other hand, takes part in the catalytic mechanism of CDK-2 about phosphorylation of the target protein. Ligand interactions with these residues change the activity of CDK-2, which can activate or inhibit the cell cycle in cancer cells [29,30].

Inhibitors made to target these areas can stop CDK-2 from working, which helps to prevent cancer cells from growing, especially in hormone receptor-positive breast cancers. The functional implications of this interaction are profound. Blocking CDK-2 through the interaction with Asp145 and His84 may arrest the cell cycle, making it potentially a useful anticancer strategy [29].

For NMDA receptor, represented by 8I0M, specific amino acids within the NR1 and NR2 subunits are crucial for the surface expression and activity of the receptor. The research has revealed that residues such as Trp-636 and Tyr-647 within the NR1 subunit and corresponding residues within the NR2 subunit play significantly in the receptor's ability to be trafficked to the cell surface as well as to bind ligand effectively [31,32]. The structural stability and interactions of such amino acids are essential for the overall function of the receptor, influencing synaptic transmission and plasticity.

For the umami taste receptor, as represented by 7PG6, residues such as Asp335, Tyr383, and Gln384 have been identified as crucial for receptor activation and ligand binding. These residues are involved in docking ligands, which enhances the receptor's response to umami compounds. Also, residues Arg-307 and Thr-172 were identified as being crucial in ligand perception and receptor stimulation [33]. These residues facilitate the binding of L-amino acids, which are important for taste. In addition, the function of the T1R1/T1R3 receptor also is controlled by specific amino acids affecting ligand-binding activity and signifying capacity, implying a close association between the structure and function of the receptor.

As for 1KV1 protein, amino acid leucine plays an important role in cancer cell metabolism and growth. L-type amino acid transporter 1 (LAT1) is responsible for transporting leucine and other essential amino acids into cells, which activates the mTOR signaling pathway crucial for cancer cell proliferation [34]. LAT1 is overexpressed in various cancers, including breast cancer, and its inhibition has shown anti-tumor effects.

Interestingly, leucine deprivation or inhibition of leucine uptake has demonstrated potential as a therapeutic strategy against breast cancer. For example, inhibiting LAT1 using JPH203 suppressed cell proliferation, migration and invasion in bladder cancer cells [34]. Similarly, inhibiting LAT function in prostate cancer cells led to suppression of mTOR signaling and cell cycle progression.

In breast cancer specifically, leucine limitation impaired mTORC1 activity in tumor-infiltrating lymphocytes, suggesting leucine supplementation could potentially improve anti-tumor immunity when combined with immunotherapy. Additionally, the leucine transporter SLC7A5 was found to be crucial for endocrine therapy resistance in ER+ breast cancer, identifying it as a potential therapeutic target [35-37].

C. aurantiifolia peel extract preparation

Through a systematic approach to our daily progress assessments, we significantly enhanced both the yield and potency of our extract by meticulously fine-tuning various parameters. The resulting peel extract showcased a striking vibrancy in color and an enticing aroma, coupled with a remarkable concentration of beneficial phytochemicals. This careful methodology not only amplified the extract's effectiveness but also laid a robust groundwork for future research and development endeavors, promising exciting possibilities in product innovation.

In order to guarantee comprehensive extraction, we macerated the material in ethanol for 3 consecutive 24-h periods following its pulverization into a fine powder. We then filtered the mixture to obtain the filtrate, which we then concentrated using a rotary evaporator set at 40 °C. This method yielded a concentrated ethanol extract. In order to evaluate the efficacy of our extraction, we determined the extract yield by dividing the mass of the extract by the initial mass of the *C. aurantiifolia* fruit peel used. This calculation established a firm foundation for the evaluation of our results.

$$\text{Extract Yield} = \frac{\text{mass of extract obtained}}{\text{mass of } C.aurantiifolia \text{ fruit peel used}} \times 100\% \quad (1)$$

We effectively obtained the concentrated ethanol extract, enabling a comprehensive assessment of our extraction method's efficiency and the application of the extraction yield formula. This quantitative evaluation not only emphasizes the efficacy of our methodology but also provides a solid foundation for the subsequent examination of the extract's properties and potential applications. The rigorous methodology in this study underscores the significance of our findings in the investigation of *C. aurantiifolia* peels utilization, further enhancing its credibility. We have conducted a thorough evaluation of our extraction method's efficiency and applied the extraction yield formula. This quantitative analysis highlights the effectiveness of our approach and lays a strong foundation for future studies on the properties and possible applications of the extract. The importance of our findings regarding the use of *C. aurantiifolia* peels is reinforced by the meticulous methodology utilized in this research, which bolsters its credibility.

Microencapsulation of *C. aurantiifolia* peel extracts

The process involves microencapsulating *C. aurantiifolia* peel extracts. We carried out the microencapsulation of the extract with modifications based on the literature [12]. First, 2.8 g of gelatin was dissolved into 140 mL of distilled water and stirred with a magnetic stirrer at 60 ± 1 °C and a stirring rate of 600 rpm. Next, proceed to incorporate 5 mL of varying extract into the mixture. Next, we added gum arabic solution, drop by drop, up to 40 mL (varied), at a concentration of 2%.

Next, we stirred the beaker containing the solution for 15 min at 60 °C and then added 2.5% (v/v) glacial acetic acid solution to adjust the pH of the mixture to 3.75. The solution was cooled to 10 °C. Microcapsules formed in the solution were added to 0.066% glutaraldehyde as much as 475 µL (varied). We raised the temperature of the solution to 35 °C and continued stirring for 3 - 4 h to complete the crosslinking reaction. We then cooled the solution to room temperature while stirring it. We filtered the microcapsules using a Buchner funnel and then washed them with water. We dried the microcapsules in a desiccator. We carried out this procedure in triplicate for all the different extracts.

Microcapsule characterization of *C. aurantiifolia* peel extract

By looking at their chemical and physical properties, we can find out how stable microcapsules are that contain *C. aurantiifolia* peel extract, how they release the extract, and what they could be used for. This process is essential for optimizing the use of the extract in various fields, such as food preservation or pharmaceutical formulations.

Microcapsule yield

The yield refers to the quantity of microcapsules produced during the encapsulation process. This is a crucial factor in figuring out how well and whether it is possible to use *C. aurantiifolia* peel extract in business. A higher yield indicates better utilization of the extract and can lead to more cost-effective production methods. We determine the microcapsule yield by dividing the obtained mass of microcapsules by the total mass of reactants used. The equation serves as the foundation for calculating the microcapsule yield.

$$\text{Microcapsule Yield} = \frac{\text{mass of microcapsules obtained}}{\text{total mass of reactants used}} \times 100\% \quad (2)$$

Researchers can quantify the efficiency of the microencapsulation process with this formula, gaining insight into the effective transformation of reactants into microcapsules. A higher yield percentage indicates a more successful encapsulation, which is crucial for evaluating the potential applications of the extract.

Encapsulation efficiency (EE)

This crucial metric evaluates the efficiency of ensnaring the intended substances in the microcapsules. This measurement not only assesses the success of the encapsulation process but also informs potential improvements for future formulations. We calculated the encapsulation efficiency (EE) by dividing the extract content in the microcapsules by the total amount of extract added in the formulation. The calculation of encapsulation efficiency (EE) utilizes the following equation:

$$\%EE = \frac{\text{extract content in microcapsules}}{\text{amount of extract added}} \times 100\% \quad (3)$$

This formula quantifies the effective incorporation of the extract into the microcapsules. A higher EE percentage indicates a successful encapsulation of a larger proportion of the initial extract, crucial for its intended use in various applications.

Extract content (EC)

This metric measures the actual amount of the extract successfully contained within the microcapsules following the encapsulation process. This metric is crucial for assessing the effectiveness of the encapsulation method and guaranteeing the preservation of the extract's desired properties for its intended use. We determined the extract content (EC) by dividing the extract content in microcapsules by the total weight of the microcapsules produced. The EC calculation relies on the following equation:

$$\%EC = \frac{\text{extract content in microcapsules}}{\text{weight of microcapsules}} \times 100 \quad (4)$$

This formula provides a clear measurement of how much of the microcapsules' weight consists of the extract, allowing for assessment of the efficiency of the encapsulation process. A higher EC value indicates a more effective use of materials, which is vital for optimizing product formulation.

PSA (particle size analyzer)

Researchers use the instrument to determine the size distribution of the microcapsules, which can influence their release properties and overall performance in applications. By analyzing particle size, researchers can further refine the encapsulation process to enhance the effectiveness of the product.

We suspended a dry sample of 0.5 g in 10 mL of dispersant. If the suspension was clumpy, we added additional dispersant. We then put the suspension into a magnetic stirrer or vortex mixer to even out the initial distribution. Next, we perform ultrasonication for 1 - 5 min, depending on the sample's nature, to break agglomerates and disperse the particles optimally. After that, we load the sample into the PSA instrument by taking a homogeneous suspension from the center. We produce a diagram of particle size distribution based on light scattering (laser diffraction or dynamic light scattering).

Fourier transform infrared (FTIR) spectroscopy

We then utilize this method to scrutinize the chemical makeup of the particles. This technique provides valuable insights into the molecular structure and functional groups present, enhancing our understanding of the sample's properties.

We took a sufficient amount of the dry sample, added KBr at a 1:10 ratio, and pulverized it. Next, we pressed the sample under high pressure to form a pellet. After inserting the pellet into the FTIR instrument, the resulting spectrum revealed the percentage transmittance (%T) from wave numbers 400 - 4000 cm^{-1}. The equation uses this transmittance value to identify the functional group, as molecules absorb infrared energy at specific wavelengths, leading to a decrease in transmittance (%T) at that wavelength.

$$A = -\log\left(\frac{\%T}{100}\right) \quad (5)$$

The provided equation establishes a relationship between the absorbance (A) and the percentage transmittance (%T), suggesting that when molecules absorb infrared energy, the absorbance rises and the transmittance falls. This relationship is crucial for analyzing the functional groups present in the sample based on their characteristic absorption patterns.

Thermogravimetry analyzer (TGA)

The technique used to measure changes in a material's weight as it is heated, cooled, or held at a constant temperature, which can provide insight into the thermal stability and composition of the sample. By combining TGA with infrared spectroscopy, researchers can correlate weight loss events with specific functional groups, enhancing the overall analysis.

We took a dry sample of at least 10 mg. Next, we insert the dry sample into a TGA instrument, set to a temperature range of 25 - 960 °C, a heating rate of 10 °C/min, and an N_2 inert gas for material decomposition. The analysis yields a spectrum that illustrates the material's decomposition within a typical temperature range of the sample's constituent materials.

Scanning electron microscopy (SEM)

The instrument provides detailed images of the sample's surface morphology and structure. This complementary technique allows for a deeper understanding of the material's characteristics and behavior during the thermal analysis. We took a sufficient number of dry samples and coated them with Pt metal using a sputter coater. Next, we glued the sample to the SEM stub using carbon tape. Next, we set the accelerating voltage (5 - 20 kV) and analyzed an image of the sample's surface structure.

Release rate mechanisms and kinetics

The processes that control the speed and pattern of a substance's release over time are known as the release rate mechanism and kinetics. Understanding these mechanisms is crucial for optimizing drug delivery systems and other applications where controlled release is essential.

We used a sonicator to observe the release of *C. aurantiifolia* extract. We weighed the resulting microcapsules up to 0.25 g and dissolved them into 10 mL of ethanol. We used a sonicator to stir the microcapsule and ethanol mixture at a constant rate and temperature for 120 min. We pipetted 3 mL of the ethanol sample every 15 min to analyze it using a UV-Vis spectrophotometer at a wavelength of 316 nm, determining the percentage of extract that emerged over 2 h. We returned the sample after each test to maintain a constant volume. We then conducted a statistical analysis using Oneway ANOVA to determine the release mechanism.

To elucidate the dynamics of extract release from microcapsules, various release kinetic models were evaluated, including the Avrami model (expressing the fraction of the microcapsule that has changed from the initial phase to the final phase as a function of time), zero-order (representing the percentage of extract released over time), first order (describing the logarithmic relationship between the percentage of extract remaining and time), Higuchi model (measuring the percentage of extract release against the square root of time), Hixson-Crowell model (detailing the cubic root relationship of extract remaining over time), and Korsmeyer-Peppas model (establishing a logarithmic relationship between the percentage of extract released and time) [38].

Results and discussion

***In silico* analysis and molecular docking**

Microcapsules represent one of the new drug delivery systems under extensive development to improve the efficacy and efficiency of therapy in various diseases, including cancers. In this effort, extending this application to breast cancer, an attempt will be made to develop microcapsules for adjuvant therapy in the following study. The article deals with a computer-based study on some potential interactions of microencapsulated bioactive compounds with certain key proteins within the MCF-7 breast cancer cells.

Earlier research indicated the existence of 10 major compounds (compounds 1- 5 Julaeha *et al.* [12] and compounds 6 - 10 Permadi *et al.* [27]) and 9 isolated compounds (compounds 11 - 13 Julaeha *et al.* [11] and compounds 14 - 19 Wilson *et al.* [25]) that were obtained successfully from *C. aurantiifolia* peel extract. The literature then paired 19 compounds with 3ERT, 3PY0, 8I0M, 7PG6, and 1KV1 receptors.

The docking results obtained (**Table 1**) showed possible binding affinities that may influence the design of new therapeutic agents. It is based on this premise that such phytochemicals found in *C. aurantiifolia* peel might be contributing their own to modulating the biological activities of these receptors.

Table 1 The binding affinity of natural ligands and the main compound of *C. aurantiifolia* as potential ligands.

		3ERT	CDK2 - 3PY0	CDK4 - 8I0M	PI3K - 7PG6	MAPK - 1KV1
	RMSD	1.1128	1.4402	0.4918	0.6466	0.5651
	Nature ligand (Estradiol)	−9.556				
No.	Nature ligand (SU9516)		−8.299			
	Nature ligand (computated)			−9.713		
	Nature ligand (computated)				−9.027	
	Nature ligand (computated)					−8.550
1	Murrayacarpin A	−6.928	−7.649	−6.759	−6.269	−6.295
2	2,4,4′,6′-Tetrahydroxybenzophenone	−7.747	−8.325	−7.314	−7.713	−7.073
3	Evodin	−9.909	−7.353	−6.999	−9.228	−7.622
4	Bergaptol	−7.506	−8.351	−7.508	−7.315	−6.444
5	Crocetin	−8.196	−8.705	−8.588	−7.646	−8.383
6	Nobiletin	−7.028	−8.270	−6.857	−6.779	−6.978
7	Tangeretin	−7.137	−8.443	−7.627	−6.768	−7.052
8	Scoparone	−6.557	−7.305	−6.774	−6.416	−5.925
9	Sinensetin	−7.345	−8.987	−7.482	−7.101	−7.205
10	Tetramethylscutellarein	−7.020	−8.677	−7.649	−7.262	−7.043
11	5-Geranyloxy-7-methoxy coumarin	−7.827	−9.404	−7.832	−7.240	−8.793
12	5-Geranyloxypsoralen	−8.330	−9.767	−9.012	−7.777	−8.716
13	8-Geranyloxypsoralen	−8.522	−8.433	−9.524	−7.803	−8.346
14	Methyl isolimonate acetate	−8.401	−5.930	−7.423	−7.693	−7.073
15	Europetin	−6.876	−9.052	−8.088	−7.608	−7.703
16	Luteolin	−8.388	−9.660	−8.916	−8.048	−8.337
17	Limonin	−9.408	−7.484	−7.430	−8.629	−7.817
18	3`-Hydroxygenkwanin	−7.664	−9.536	−8.627	−8.087	−8.269
19	Myricetin	−7.196	−9.030	−8.129	−7.831	−7.788

A 3ERT and 3PY0 nature ligand (estradiol and SU9516) were used as a reference ligand. Meanwhile, 8I0M, 7PG6, and 1KV1 nature ligand obtained by computation calculation. The ligands with potency greater than the estradiol, SU9516, and computated natural ligands were selected for further analysis as shown in **Table S1**.

Overall, only evodin (3) out of 19 screened ligands showed strong interactions with the 3ERT protein; 2,4,4′,6′-tetrahydroxybenzophenone (2), bergaptol (4), crocetin (5), tangeretin (7), sinensetin (9), tetramethylscutellarein (10), 5-geranyloxy-7-methoxy coumarin (11), 5-geranyloxypsoralen (12), 8-geranyloxypsoralen (13), europetin (15), luteolin (16), 3`-hydroxygenkwanin (18), myricetin (19) out of 19 screened ligands showed strong interactions with the 3PY0 protein; and only 5-geranyloxy-7-methoxy coumarin (11) and 5-geranyloxypsoralen (12) out of 19 screened ligands showed strong interactions with the 1KV1 protein with good docking score as shown in **Table 1** and better interaction as shown in **Table S1**.

Evodin (3) showed a van der Waals interaction with Asp351, which is a major amino acid of the 3ERT protein. In the case of the 3PY0 protein, there was a connection through van der Waals and hydrogen bonds with 2 important amino acids, Asp145 and His84, interacting with compounds like 2,4,4',6'-tetrahydroxybenzophe-

none, bergaptol, crocetin, tangeretin, sinensetin, tetramethylscutellarein, 5-geranyloxy-7-methoxy coumarin, 5-geranyloxypsoralen, 8-geranyloxypsoralen, europetin, luteolin, 3`-hydroxygenkwanin, and myricetin. For the case of 1KV1 protein, there was no information on the major amino acids that play crucial roles. Still, in the ligand-to-receptor interaction, it can be seen a connection through van der Waals and alkyl interaction with Leu167.

The calculated ligand affinities were within the range of −6.269 to −9.909 kcal/mol. Evodin (3) had a higher value, −9.909 kcal/mol, compared to 3ERT nature ligand, estradiol, at −9.556 kcal/mol. Other compounds showing their better binding strengths were 2,4,4',6'-tetrahydroxybenzophenone (2), bergaptol (4), crocetin (5), tangeretin (7), sinensetin (9), tetramethylscutellarein (10), 5-geranyloxy-7-methoxy coumarin (11), 5-geranyloxypsoralen (12), 8-geranyloxypsoralen (13), europetin (15), luteolin (16), 3`-hydroxygenkwanin (18), myricetin (19) with a value of −8.325, −8.351, −8.705, −8.443, −8.987, −8.677, −9.404, −9.767, −9.052, −9.660, −9.536, and −9.030 kcal/mol. All of these have higher binding strengths than their natural ligand, SU9516, which is −8.299 kcal/mol. Meanwhile, 5-geranyloxy-7-methoxy coumarin and 5-geranyloxypsoralen show better binding strength with values of −8.793 and −8,716 kcal/mol than 1KV1 computational nature ligand binding value of −8.550 kcal/mol. Ligand efficiency, which is the ability of a compound to produce the desired clinical effect, is equal to ligand affinity and thus useful during optimization.

Ligand efficiency decides on the perfect interaction between ligand and receptor. It is the ratio of Gibb's free energy (ΔG) to nonhydrogen atoms of the compound. It measures the binding energy of every atom of a ligand that binds to a receptor or enzyme. The lesser the Gibbs free energy, the more spontaneous the interaction between the ligand-receptor binding. The stronger the ligand binds to the receptor, the more potent the inhibitory effect is to the natural ligand. Different functional groups in the structure of the ligands, including a side chain and hydroxyl groups, account for the difference in their binding affinities. Molecular docking analysis categorizes the ligands according to the best binding position and higher affinity values in the negative, followed by further analyses on the stability of each inside the protein binding pocket.

***C. aurantiifolia* peel extract preparation results**

We prepared the *C. aurantiifolia* peel extract by macerating it with ethanol solvent; we then filtered and concentrated the macerate to produce a concentrated extract. We used 10 kg of *C. aurantiifolia*, which gave 398.8 g of peel simplisia and 45.4752 g of ethanol-concentrated extract, for a yield of 11.4%. Indriyani *et al.* [10] found that the average yield of ethanol extract from the skin of *C. aurantiifolia* ranged from 1.67% to 5.24%, indicating a good yield. In contrast, the yield of 11.4% exceeded the good indicator. We determined the maximum wavelength of the concentrated extract and created a standard curve for further purposes, including determining %EE, %EC, and the optimal formulation of microcapsules. The maximum wavelength obtained was 316 nm, with the standard curve obtained having an R^2 of 0.9999, which means that the linear regression is nearly perfect.

Microencapsulation

This process encapsulates active substances within a coating material to protect them and control their release. This technique enhances the stability and efficacy of the encapsulated compounds, making them ideal for various applications in pharmaceuticals and food technology. Therefore, we need to optimize the ratio between the extract as the active substance, gelatin-gum arabic as the coating matrix, and glutaraldehyde as the crosslinker.

Variation of extract-to-matrix ratios

The variations of extract-to-matrix ratios are crucial for optimizing the encapsulation process, as they can influence the efficiency and stability of the microcapsules. By adjusting these ratios, we can enhance the overall performance of the formulation in terms of release and bioavailability.

We carried out variations in the extract: matrix ratio in this study to produce optimum microcapsules. **Table 2** illustrates the variations in the extract ratio used. After obtaining the data, statistical clustering was performed using Oneway ANOVA with significant differences if $p < 0.05$.

Table 2 Microencapsulation formulation of various extract concentrations.

Formulation Code	Extract Concentration (%w/v)	Yield (%)	%EE	%EC
E 1	0.55	33.55 ± 1.28^{c}	97.89 ± 0.93^{a}	0.87 ± 0.01^{d}
E 3	1.64	44.94 ± 4.72^{b}	98.40 ± 1.09^{a}	1.85 ± 0.13^{c}
E 5	2.70	44.16 ± 5.85^{b}	99.18 ± 0.80^{a}	3.16 ± 0.36^{a}
E 7	3.74	54.21 ± 3.36^{a}	99.65 ± 0.09^{a}	3.67 ± 0.24^{a}
E 9	4.76	46.19 ± 6.69^{b}	50.27 ± 9.66^{b}	2.65 ± 0.23^{b}

Ratio of gelatin: gum arabic dressing 2:2, $p < 0.05$

Yield

Table 2 indicates that increasing the concentration of extract improves the yield produced. The yield produced was within the range of 33.55 - 54.21%. It produced the highest yield of 54.21±4.76% when 3.74% extract was mixed with a dressing of 2:2 gelatin to gum arabic and 0.066% glutaraldehyde crosslinker in as much as 475 µL of dressing.

The optimum yield produced is statistically significantly different from the best results in Group (a). This would mean that the concentration of the optimized extract leads to a more efficient process. Other further studies can be the variation of ratios and crosslinker which of those will lead to efficiency and a higher yield of output.

Extract content

The parameter known as extract content (EC) determines the core ratio of bioactive substances suitable for capsule coating to the microcapsules produced, also known as the load capacity. EC signifies the optimal ratio of extracts that the matrix can coat. The resulting EC varied from 0.87 to 3.67%, depending on the coating matrix used.

Increasing the extract concentration from 0.55 to 3.74% (w/v) led to an increase in extract content (%EC), whereas further increase to 4.76% resulted in a decrease. Statistical analysis showed significant differences among the formulations (E1–E7), with Group (a) showing the highest %EC, which was significantly different from Group (b) ($p < 0.05$).

Although formulations E5 and E7 were both included in Group (a), indicating no significant difference in %EC, further evaluation was necessary to determine the optimal formulation. Considering additional parameters such as yield and encapsulation efficiency (%EE), formulation E7 demonstrated the best overall performance. At an extract-to-matrix ratio of 3.74:4, the addition of 0.07 g of extract resulted in the most optimal microcapsule characteristics.

Encapsulation efficiency

Encapsulation efficiency (EE) is defined as the ratio of the mass of the core material completely trapped in the coating material to the mass of the core material used in the formulation. The encapsulation process will yield the highest %EE if the coating matrix completely traps almost all bioactive substances. Thus, the technology succeeds in providing maximum protection to the bioactive substances.

The addition of extracts with a concentration of 0.55-3.74 (%w/v) to the coating did not show a significant increase in %EE. The statistical test reveals a significant increase in %EE in one Group (a). Meanwhile, the addition of extract concentration 4.76:4 to the dressing showed a decrease in %EE with a significant difference in Group (b).

The highest %EE resulted from formulation code E7, 99.65±0.09%, meaning that 99.65% of the 0.07 g extract added was successfully coated by the matrix used. Therefore, we concluded that the optimum extract: matrix ratio is at a value of 3.74:4, allowing us to continue the study with the addition of 0.07 g of extract.

The findings indicate that the formulation code E7 achieved the highest encapsulation efficiency, with an impressive $99.65 \pm 0.09\%$. This indicates that the matrix effectively coated nearly all of the 0.07 g incorporated extract, highlighting the potential of this formulation. Consequently, we determined that the optimal extract-to-dressing ratio is 3.74:4, which enables us to proceed with further investigations using the same amount of extract.

Variation of crosslinker ratios

Once we determined that adding an extract at a concentration of 3.74:4 to the dressing yielded the highest yield, %EC, and %EE, we proceeded with a second variation, the crosslinker. The crosslinker plays a crucial role as it enhances the solvent's interaction with the matrix's pores, allowing the extract to escape from the microcapsules. **Table 3** illustrates the variations in the crosslinker used. After obtaining the data, statistical clustering was performed using Oneway ANOVA with significant differences if $p < 0.05$.

Table 3 Microencapsulation formulation of various crosslinker concentration.

Formulation Code	Glutaraldehyde Concentration (%w/v)	Yield (%)	%EE	%EC
375	0.052	14.95 ± 0.71^{b}	38.75 ± 2.11^{c}	4.94 ± 0.07^{a}
425	0.059	24.49 ± 1.38^{b}	50.49 ± 4.85^{b}	4.85 ± 2.81^{a}
475	0.066	54.21 ± 3.36^{a}	99.65 ± 0.09^{a}	3.67 ± 0.24^{a}
525	0.073	9.33 ± 0.21^{b}	34.01 ± 0.02^{c}	6.95 ± 0.21^{a}
575	0.080	9.54 ± 1.28^{b}	25.09 ± 0.08^{d}	5.16 ± 1.23^{a}

Ratio of extract to dressing 3.74:4, $p < 0.05$

Yield

Table 3 indicates that adding more glutaraldehyde as a crosslinker initially raised the yield from 14.95% to 54.21% when the amount ranged from 0.052% to 0.066%. However, after reaching a peak, the yield began to decrease. When too much glutaraldehyde was added (0.073% - 0.080%), the yield dropped to 9.33% - 9.54%. This shows that using too much glutaraldehyde can harm the crosslinking process and reduce the quality of the final product. This suggests a need for careful optimization of crosslinker concentration to achieve the best results in future experiments.

According to the tests, formulation code 475 had the best results in Group (a), achieving a high yield of 54.21 ± 4.76%. This was obtained by adding 475 µL, or 0.066%, of glutaraldehyde to the extract and the gelatin-gum arabic dressing. The test results show that using 0.066% glutaraldehyde gives the best amount of coated extract. Using more than 0.066% glutaraldehyde leads to a lower yield. The destruction of polymer integrity due to overly rigid bonds is the cause of this decrease, which led to the identification of formulation code 475 as the optimal formula.

Extract content

The statistical test, which showed that the entire variation was in Group (a), indicated that the addition of glutaraldehyde at a concentration of 0.052% - 0.080% did not significantly increase the EC.

Statistical analysis based on yield and %EE reveals that only formulation code 475, with a glutaraldehyde addition of up to 0.066%, has overall significance in Group (a). This implies that the optimal ratio for crosslinking is 0.066 to the extract: gelatin-gum arabic dressing 3.74:4. This optimal ratio not only enhances the mechanical properties of the dressing but also ensures better stability and sustained release of the active compounds.

Encapsulation efficiency

The addition of glutaraldehyde at a concentration of 0.052% - 0.066% significantly increased the %EE, with statistical testing showing an increase from Group (c) to Group (a). Meanwhile, the addition of glutaraldehyde at a concentration of 0.073% - 0.080% did not yield the best results, leading to a decrease in Groups (c) and (d). This indicates that while a small concentration of glutaraldehyde enhances the encapsulation efficiency, higher concentrations may have an adverse effect. Consequently, finding the optimal concentration is crucial for achieving the desired results.

The %EE significantly decreases when the glutaraldehyde concentration exceeds 0.066%,

indicating that the matrix's coating ability reaches its peak at 0.066% glutaraldehyde addition. This suggests that there is a threshold for glutaraldehyde concentration, beyond which the encapsulation efficiency diminishes. Therefore, maintaining the concentration around 0.066% is essential for maximizing the effectiveness of the encapsulation process.

In conclusion, formulation code 475 is the best when it includes 475 µL of glutaraldehyde, which is 0.066%, mixed with the dressing made of extract, gelatin, and gum arabic in a ratio of 3.74:2:2.

Variation of matrix ratios

The final experiment involves adjusting the dressing ratio, utilizing 2 types of dressings: gelatin and gum arabic, and optimizing this ratio to yield the optimal microcapsules. This step is crucial because the correct ratio of gelatin to gum arabic will influence the structural integrity and release characteristics of the microcapsules. Therefore, fine-tuning this ratio is essential for achieving optimal performance in the final product.

This variation involves fixing the concentration of one dressing while varying the concentration of the other dressing. **Table 4** shows that we fixed the concentration of gelatin and varied the gum arabic. After obtaining the data, statistical clustering was performed using Oneway ANOVA with significant differences if $p < 0.05$.

Table 4 Microencapsulation formulation of various dressing concentrations.

Formulation Code	Gum Arabic Concentration (%w/v)	Yield (%)	%EE	%EC
GA 20	1	13.68 ± 1.69^{c}	31.34 ± 0.18^{c}	3.59 ± 0.31^{a}
GA 30	1.5	43.38 ± 2.04^{b}	67.73 ± 0.13^{b}	3.37 ± 0.11^{a}
GA 40	2	54.21 ± 3.36^{b}	99.65 ± 0.09^{a}	3.67 ± 0.24^{a}
GA 50	2.5	79.90 ± 4.91^{a}	99.74 ± 0.20^{a}	2.32 ± 0.11^{b}
GA 60	3	86.91 ± 8.22^{a}	99.83 ± 0.13^{a}	2.00 ± 0.16^{b}

Ratio of extract to gelatin 3.74:2, $p < 0.05$

Yield

Table 4 reveals that the addition of gum arabic concentration boosted the yield within the range of 13.68 - 86.91%. However, statistical tests on %EE and %EC showed that formulation code GA 40 had the highest yield of 54.21 ± 4.76% in Group (a). This was achieved by adding 2:2 gum arabic to gelatin and 0.06% glutaraldehyde crosslinker in 475 µL.

This indicates that the encapsulated extract reaches its maximum at a concentration of 2% gum arabic, while concentrations above 2% result in an increased yield due to the formation of empty microcapsules without extracts. Therefore, we identify the formulation code GA 40 as the optimal formula.

Extract content

The addition of a gum arabic concentration of 1:2-2:2 to the gelatin resulted in an increase in the %EC, but it did not show a statistically significant difference within the same Group (a), whereas Group (b) experienced a difference of 2.5:2 - 3:2. Formulation code GA 40 gave the best %EC of 3.67 ± 0.24% in Group (a) with 2% gum arabic added, meaning that the best ratio obtained for the dressing was 2:2. While the addition of gum arabic improved the %EC in Group (a), the 2:2 ratio proved to be the most effective formulation, demonstrating optimal performance under those specific conditions. Conversely, Group (b) showed a more pronounced difference, suggesting variations in response to the formulations tested.

Encapsulation efficiency

The addition of gum arabic at a concentration of 2:2 - 3:2 (%b/v) to gelatin did not show a significant increase in %EE. However, statistical testing showed that the %EE was in the best category, i.e., Group (a). Meanwhile, adding a gum arabic concentration of 1:2 - 1.5:2 to gelatin did not show the best results in Groups (b) and (c).

It didn't make a difference in the %EE when more gum arabic was added than the 2:2 ratio. This means that the matrix's binding power was at its best when 2% gum arabic was added. The yield increased as the gum arabic concentration increased without a corresponding increase in %EE, indicating the formation of empty capsules devoid of extract.

The exploration of gum arabic's role in enhancing gelatin matrix binding reveals a nuanced relationship that underscores the importance of concentration and formulation ratios. While the 1:2 - 1.5:2 ratios did not produce optimal outcomes in Groups (b) and (c), it became evident that a 2% addition of gum arabic significantly bolstered the binding power of the matrix, demonstrating its potential for improving encapsulation efficiency. However, this beneficial effect was tempered by the observation that increasing the concentration further resulted in empty capsules, indicating a threshold beyond which additional gum arabic fails to contribute positively to extract retention. These findings emphasize the delicate balance required in formulating gelatin-based systems and highlight gum arabic's critical role as both an enhancer and a limiting factor in achieving desired encapsulation outcomes.

Based on the experimental results, the extract:gelatin:gum arabic:glutaraldehyde ratio of 3.74:2:2:0.066 was selected through optimization of encapsulation efficiency, microcapsules yield, and extract content, rather than on bioactivity equivalence to specific phytochemicals. This optimized formulation was subsequently subjected to further characterization, as outlined in the introduction, to evaluate its structural, thermal, morphological, and release properties.

Functional group analysis

The FTIR analysis results can shed light on the functional groups present in the microcapsules (**Figure 1**). The hydroxyl groups in gelatin-gum arabic and gelatin-gum arabic-glutaraldehyde cause the O-H stretching, as indicated by the peaks between 3600 and 3200 cm^{-1}. The peak at 1680 - 1690 cm^{-1} is a common value for an amide bond made from NH_2 groups in gelatin and C=O in glutaraldehyde. The peaks at 1250 - 1000 and 1150 - 1050 cm^{-1} show typical wave numbers for the C-N and C-O strains. All of these peaks sum up in the **Table 5**.

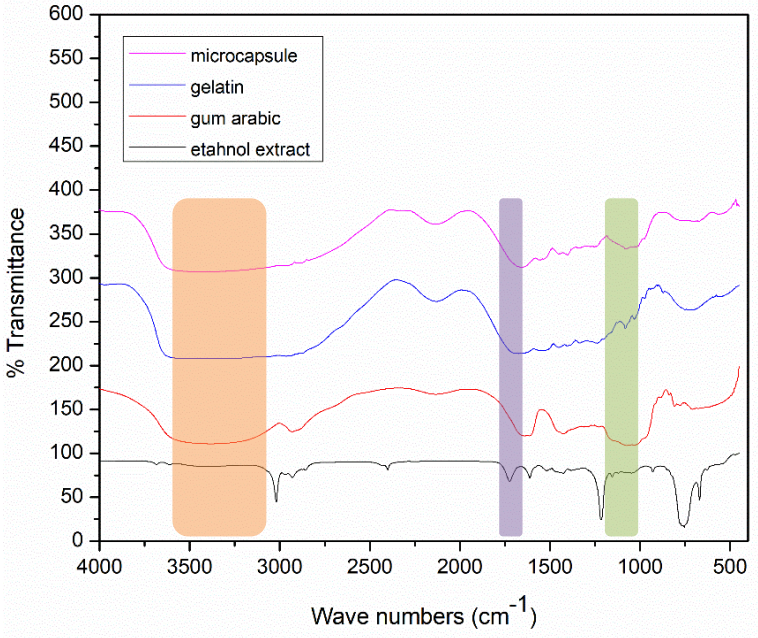

Figure 1 FTIR spectrum of microcapsules, gelatin, gum arabic, and ethanol extract of *C. aurantiifolia.*

Gelatin possesses various functional groups, especially amino groups (−NH_2), which are reactive and play a significant role in forming cross-links with glutaraldehyde, a bi-functional aldehyde that can react with these amine groups. Glutaraldehyde predominantly reacts with the free amine groups in gelatin through a nucleophilic attack, leading to the formation of stable imine or "Schiff base" linkages, which are a type of cross-link [41].

Additionally, gelatin and gum arabic can interact primarily through hydrogen bonding. Gum arabic, being a polysaccharide, has hydroxyl (−OH) groups that facilitate hydrogen bond formation with the amino and carboxyl groups present in gelatin. The electrostatic attractions and hydrogen bonding interactions are vital as they contribute to the cohesive network structure, which can be beneficial for encapsulation processes [42]

Table 5 Microcapsule functional group analysis.

Wave numbers (cm^{-1})	Prediction	Description
3600 - 3200	O−H Stretch	The interaction of hydroxyl groups on gum arabic-gelatin-glutaraldehyde
1690 - 1680	C=O Stretch	The existence of amide groups due to the interaction of NH_2 on gelatin and C=O on glutaraldehyde
1250 - 1000	C−N Stretch	The existence of electrostatic interactions of amine groups on gelatin and hydroxyl on gum arabic
1150 - 1050	C−O Stretch	

This suggests that there are electrostatic interactions between the amine groups in gelatin and the hydroxyl groups in gum arabic in the microcapsules. This means that interactions are occurring between the coating and the crosslinker.

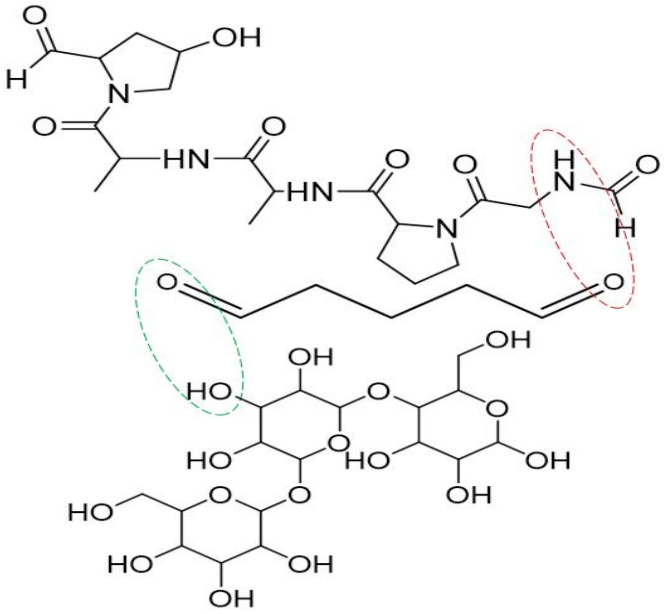

Figure 2 Gelatin-glutaraldehyde-gum arabic interaction.

These interactions, in **Figure 2**, show that glutaraldehyde, gelatin, and gum arabic work well together, which could improve the strength and effectiveness of the microcapsules. Consequently, this relationship could play a crucial role in optimizing the delivery system's performance. The absence of typical

peaks from the extract in the microcapsule spectra indicates a lack of attachment to the coating. **Figure 1** and **Table 5** illustrate this. As a result, the coating's pores allow for the controlled release of the extract from the coating without the need for any chemical reactions.

These interactions play a crucial role in the stability and functionality of the microcapsules, as they contribute to the structural integrity and release properties of the encapsulated materials, shown in **Figure 2**. Therefore, understanding these bonding characteristics is vital for optimizing the formulation and enhancing the performance of the microcapsules in various applications.

Particle size

Based on the analysis conducted using a particle size analyzer, it can be seen in **Table 6** that the microcapsules produced are in the micro range, namely 0.5 - 1000 μm, with an average value of 1.151 - 1.320 μm.

Table 6 Microcapsules particle size.

Formulation Code	Mean particle size (μm)	Mean/median ratios
GA 20	1.205 ± 0.672	1.369
GA 30	1.151 ± 0.703	1.542
GA 40	1.249 ± 0.710	1.492
GA 50	1.188 ± 0.712	1.582
GA 60	1.320 ± 0.698	0.896

When the mean/median ratio is close to 1, it indicates the heterogeneity of the produced particles. This implies a varied size distribution of the microcapsules, indicating the presence of both smaller and larger particles within the sample. A ratio near 1 signifies that the particle sizes are not uniform, which can impact the performance and application of the microcapsules. A non-uniform mashing factor can cause differences in the mixture, leading to the creation of fine powder that fits the sample requirements for the PSA instrument. This non-uniformity generates fine powder that ensures compatibility with the PSA instrument's specifications, thereby enhancing its effectiveness. On the other hand, it would be preferable to produce fine powders of the same size through an even process.

We determined the optimum formula, GA 40, based on the yield, %EE, and %EC parameters obtained. The particle size obtained from formulation code GA 40 was at a value of 1.249 ± 0.710 μm so that it fit the criteria of “microcapsules,” which is on a micro scale with a range of 0.5 - 1000 μm.

Morphology

We found that GA formulation code 40 yielded optimum results based on the parameters of yield, %EE, and %EC. We analyzed the morphology of the optimum microcapsules with formulation code GA 40 using scanning electron microscopy (SEM) and light microscopy. The analysis, as shown in **Figure 3**, revealed important structural characteristics of the microcapsules, allowing us to assess their surface features and overall quality. This information is crucial for understanding how the morphology impacts the functionality of the microcapsules in their intended applications.

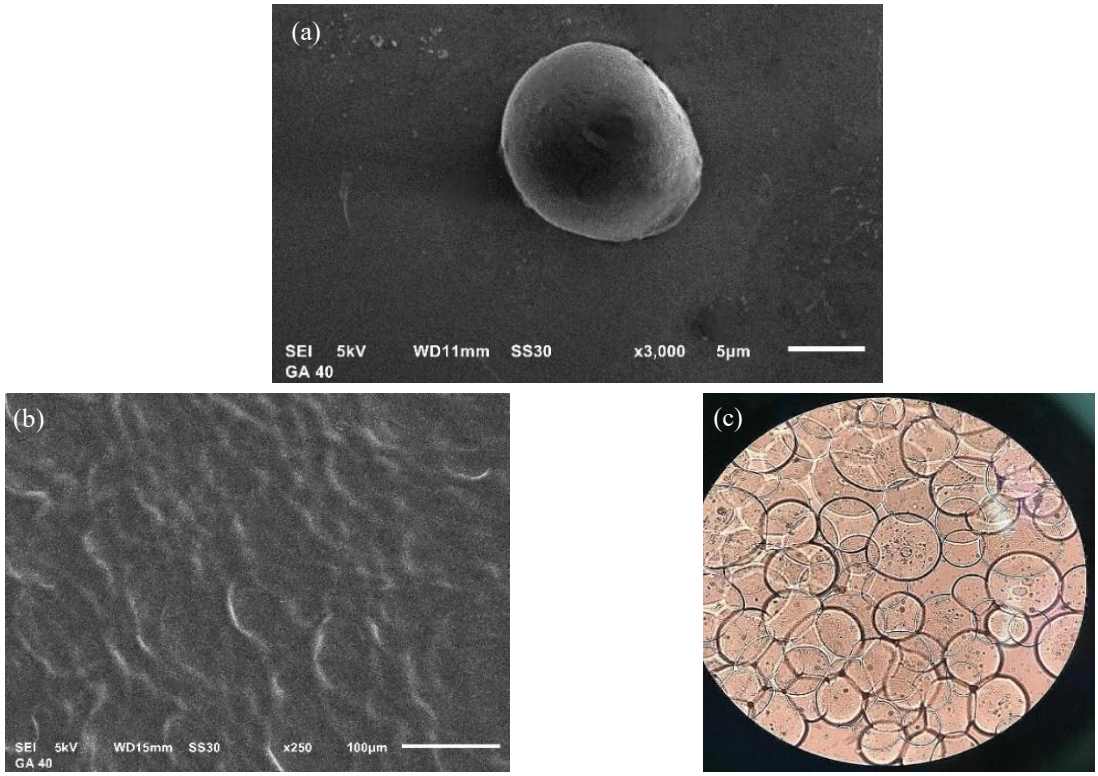

Figure 3. The morphology of microcapsules (a) under a 3000× magnification SEM, (b) under a 250× magnification SEM, and (c) under a 400× magnification light microscopy.

Uneven stirring and natural properties such as surface tension and thickness can result in irregular shapes within the microcapsules, preventing them from being perfectly round, despite their mostly spherical appearance and slightly flat surfaces. However, it is essential to consider that the observed irregularities in microcapsule morphology might not significantly impact their functional performance. Additionally, variations in formulation conditions could lead to different morphological characteristics that may still achieve desirable outcomes in specific applications.

Thermal stability

Thermal stability is an important feature in the process of protecting bioactive compounds. Thermal stability indicates the extent of particle degradation upon heating [39]. Microcapsules must be able to withstand high temperatures in order to control extract loss. The thermal decomposition of polysaccharides happens in several steps. A thermogravimetry analyzer (TGA) can measure this thermal stability. First, physically absorbed water is removed. Dehydration then releases some water molecules. Finally, the breakdown of C-O and C-C bonds occurs, which produces carbon monoxide (CO), carbon dioxide (CO_2), and water (H_2O) [40]. In this study, we performed TGA measurements on samples of *C. aurantiifolia* peel ethanol extract, empty microcapsules, and optimum microcapsules.

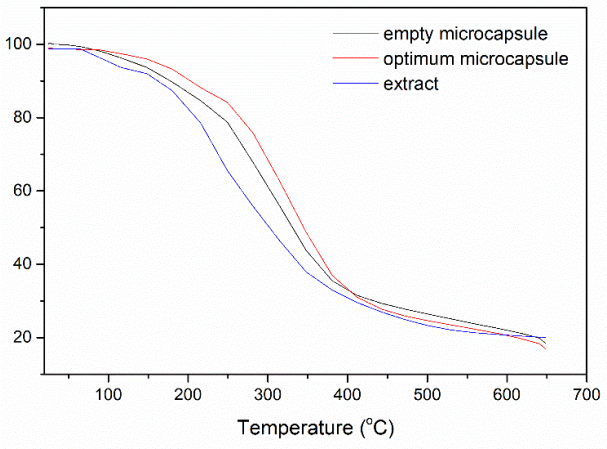

Figure 4 Thermograms of empty microcapsules, optimum microcapsules, and extracts.

The thermogram of the ethanol extract of *C. aurantiifolia* peel, as shown in **Figure 4**, showed mass changes at 3 regions of temperatures: Less than 160 °C, between 160 - 400 °C, and above 400 °C. The *C. aurantiifolia* peel ethanol extract lost 10.76 % of its mass at temperatures below 160 °C because ethanol, water, or some other substances evaporated. At 160 - 400 °C, the mass change was quite sharp, showing a loss of 62.47% of the main mass of the extract. Temperatures over 400 °C triggered the next degradation process, leaving about 25.31% of the extract intact. The extract may contain compound components that have not undergone complete decomposition, contributing to the remaining mass.

Dehydration of the water the microcapsules had adsorbed and depolymerization caused a 15.36% mass decrease in the thermogram of the optimum microcapsules at temperatures between 24.56 - 216 °C [43]. Also, the evaporation of the ethanol extract from *C. aurantiifolia* peel resulted in a weight loss of 53.10% between 216 and 411.87 °C. The key substances found in the ethanol extract of *C. aurantiifolia* peel have melting points over 200 °C. For example, bergaptol melts at 287 - 290 °C, crocetin at 286 °C, and evodin at 298 °C. The degradation of gelatin also can occur between 230 to 450 °C due to the breakdown of peptide bonds [44]. The extract's evaporation of substances that melt above 400 °C, coupled with the polymer's breakdown, resulted in an additional mass loss of 10.27% at temperatures ranging from 411.87 to 617 °C. It ends with a mass decrease of 2.73% at temperatures between 617 - 648.16 °C caused by the degradation of the remaining polymer matrix [43].

The TGA results indicate that the addition of gelatin and gum arabic coatings as microcapsules can enhance the thermal stability of the ethanol extract from *C. aurantiifolia* peel. **Figure 4** illustrates how the thermal stability of the microcapsule slows down the evaporation process of the encapsulated extract. The optimum microcapsule exhibits a graph that surpasses the extract, signifying its superior heat resistance in comparison to the uncoated extract.

Release rate and kinetics mechanism

The data showed that during the observation period of 120 min, there was an average release of 57.3954% of the extract. Therefore, because the extract does not interact with the dressing, it can gradually emerge from its pores, as illustrated in **Figure 5**.

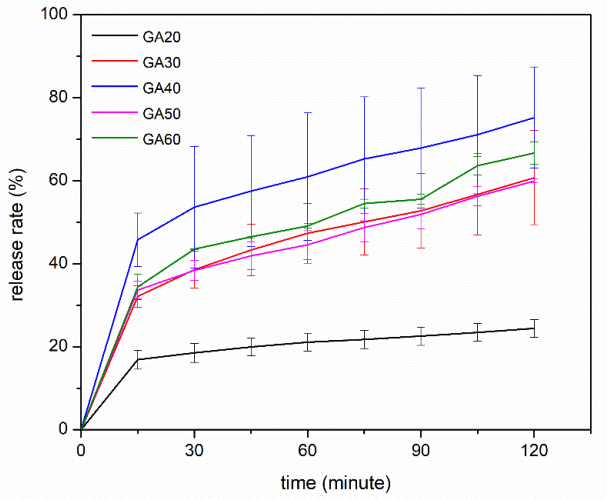

Figure 5 Graph of extract release from microcapsules.

Table 7 below links the yield, %EE, and %EC of the microcapsules to the differences in the average percentage of release for each formulation code.

We evaluated various release kinetic models to explain the dynamics of extract release from microcapsules. The analysis of **Table 8** shows that the way *C. aurantiifolia* extract is released from microcapsules follows a mix of 3 models: Higuchi, zero-order, and Hixson-Corwell.

Table 7 Release test of extracts from microcapsules.

Time (min)	Exract release (%)				
	GA 20	GA 30	GA 40	GA 50	GA 60
15	16.88 ± 2.30	32.12 ± 2.58	45.76 ± 6.48	33.65 ± 2.10	34.41 ± 3.11
30	18.50 ± 2.30	38.57 ± 4.44	53.62 ± 14.62	38.40 ± 2.42	43.52 ± 0.06
45	19.94 ± 2.17	43.32 ± 6.21	57.53 ± 13.39	41.90 ± 3.33	46.47 ± 0.18
60	21.06 ± 2.18	47.34 ± 7.22	60.97 ± 15.39	44.56 ± 3.57	49.09 ± 0.55
75	21.74 ± 2.22	50.10 ± 7.95	65.30 ± 14.93	48.73 ± 3.44	54.51 ± 1.05
90	22.53 ± 2.20	52.78 ± 9.00	67.88 ± 14.53	51.90 ± 3.47	55.55 ± 1.24
105	23.43 ± 2.15	56.70 ± 9.80	71.10 ± 14.27	56.27 ± 2.30	63.65 ± 2.23
120	24.38 ± 2.14	60.75 ± 11.33	75.23 ± 12.21	59.94 ± 0.48	66.67 ± 2.68

Table 8 Model kinetics of extract release assay from microcapsules.

Formulation Code	Total release (%)	Avrami		Korsmeyer-Peppas			Zero Order		First Order		Higuchi		Hixson-Crowell	
		R^2	k_{av}	R^2	k	n	R^2	k_0	R^2	k_1	R^2	k_{hc}	R^2	k_H
GA 20	24.38 ± 2.14^c	0.9874	0.06 ± 0.09^a	0.9889	10.331	0.1747	0.9791	0.068	0.9826	0.0004	0.9974	1.0359	0.9814	0.0012
GA 30	60.75 ± 11.33^b	0.9840	$(1.25 \pm 1.13)\times10^{-4b}$	0.9919	14.102	0.2975	0.9836	0.2557	0.9925	0.0021	0.9950	3.8828	0.9912	0.0061
GA 40	75.23 ± 12.21^a	0.9477	$(3.45 \pm 3.00)\times10^{-4b}$	0.9905	24.266	0.2304	0.9795	0.2611	0.9928	0.003	0.9954	3.974	0.9918	0.0078
GA 50	59.94 ± 2.95^b	0.9427	$(8.83 \pm 2.14)\times10^{-5c}$	0.9603	15.346	0.2729	0.9974	0.2441	0.9911	0.002	0.9796	3.6522	0.9945	0.0058
GA 60	66.67 ± 11.63^b	0.9357	$(1.49 \pm 1.10)\times10^{-4b}$	0.9662	15.128	0.3000	0.9722	0.2851	0.9681	0.0026	0.9687	4.2957	0.9722	0.0073

The slow release happens because of the strong amide bonds between the materials. This is mainly due to how the COO- groups in guluronic acid and mannuronic acid mix with the NH_2 groups in gelatin

[45]. The FTIR results support this. If the yield is low, the release percentage cannot exceed the yield, %EE, or %EC. However, changes in working conditions, such as differences in the number of samples used, can cause data anomalies, even if they are not significantly different.

The speed at which the extract emerges from the microcapsules in 120 min can significantly impact their subsequent use. For instance, when administering an anticancer drug via injection, the microcapsules must release the extract swiftly; in this scenario, formulation code GA40 is more appropriate. This way, when they reach the target area, the drug can start working on the cancer cells without delay.

Meanwhile, the released mechanism follows a mix of 3 models: Higuchi, zero-order, and Hixson-Corwell. The Higuchi kinetics model uses the obtained regression to describe the release of the active substance from the solid matrix, typically through a diffusion process. The active substance releases proportionally to the square root of time, indicating a controlled release. This kinetics model typically applies to release systems that rely on diffusion in porous matrices, making it appropriate for matrix systems with homogeneous distribution of the active substance. The FTIR spectrum confirms that the extract and the coating on the microcapsules do not interact, allowing the extract to release through the coating's pores without any chemical interaction.

Then, there are zero-order kinetics models that describe drug release at a constant rate, independent of the concentration of the active substance. This is commonly found in systems that have a release mechanism controlled by an external process, such as mechanical stimulation by a sonicator. Finally, we commonly use the Hixson-Crowell kinetics model to describe changes in particle size that impact active substance release. This kinetic model is useful for systems where dissolution and erosion of the particle surface are the main factors in active substance release.

This explanation leads to the conclusion that several kinetics models are suitable for the release of extracts from microcapsules. However, judging from the purpose of using microcapsules as breast cancer adjuvant therapy in the future, the Higuchi kinetics model is the most suitable because it describes the controlled release of extracts.

Comparative performance and therapeutic implications

The optimized extract-to-matrix ratio of 3.74:4 was selected based on a combination of encapsulation efficiency, microcapsule yield, and extract content. While the formulation was primarily guided by physical and process optimization, its therapeutic potential was also evaluated in light of bioactive compound content. Previous phytochemical studies have reported that citrus peel contains approximately 580.8 mg/kg fresh weight of quercetin, which translates to ~0.058% w/w [46]. Assuming a fivefold increase due to concentration during extraction and drying, the quercetin content in the extract may reach ~0.29%. With an extract content of 3.67% in the microcapsules, this corresponds to ~0.106 mg of quercetin per gram of microcapsules. When resuspended at 100 mg/mL, the resulting quercetin concentration is estimated to be ~35 μM, well within the reported cytotoxic range (20 - 100 μM) for breast cancer cells [47]. This projection supports the translational relevance of the selected formulation and suggests potential therapeutic utility in cancer-targeted delivery systems.

In comparison with previous studies, the encapsulation efficiency (99.65 ± 0.09%) achieved in this study is notably high. Alginate-only systems typically reach 80% - 90% EE, while maltodextrin- and sodium alginate-based systems achieve around 85% [48,49]. Gelatin-chitosan coacervates for citrus essential oils have demonstrated EE values of ~95%, and chitosan-alginate systems vary from 55% - 93%, often exhibiting Fickian-type diffusion and burst release kinetics [50]. In contrast, the current gelatin-gum arabic system maintained a controlled release profile governed by Higuchi kinetics, indicative of sustained diffusion. These results highlight the effectiveness and novelty of the complex coacervation approach employed here, which combines high encapsulation efficiency with targeted, stable release behavior suitable for natural anticancer agents.

Conclusions

This study demonstrated that *Citrus aurantiifolia* peel extract contains multiple bioactive compounds with strong binding affinities to key breast cancer proteins, as identified through *in silico* screening. Sixteen out of 95 candidate compound-protein interactions showed

significant binding, particularly with 3ERT, 3PY0, and 1KV1, indicating the extract's potential therapeutic relevance in breast cancer treatment.

To preserve the extract's bioactivity and improve its delivery, a microencapsulation system was developed using complex coacervation of gelatin and gum arabic, crosslinked with glutaraldehyde. The formulation was optimized based on encapsulation efficiency, extract content, and yield. The best-performing formulation consisted of an extract:gelatin:gum arabic:glutaraldehyde ratio of 3.74:2:2:0.066, which produced spherical microcapsules with an average diameter of 1.249 ± 0.710 μm, a high encapsulation efficiency ($99.65 \pm 0.09\%$), extract content ($3.67 \pm 0.24\%$), and yield ($54.21 \pm 4.76\%$).

Release studies confirmed Higuchi-controlled diffusion, supporting a sustained release mechanism. Based on estimated quercetin content (580.8 mg/kg fresh weight) and microcapsule formulation, the system is projected to deliver quercetin at ~35 μM—within the cytotoxic range for breast cancer cells—when resuspended at 100 mg/mL. This further supports the translational potential of the microencapsulated extract.

Overall, the findings highlight the novelty and effectiveness of the gelatin–gum arabic coacervation system in delivering *C. aurantiifolia* peel extract as a stable, targeted anticancer agent. Future work will focus on compound-specific quantification and *in vitro* cytotoxicity assays to validate the therapeutic relevance and delivery efficiency of the microcapsules for use in adjuvant breast cancer therapy.

Acknowledgments

The authors gratefully acknowledge the support of Universitas Padjadjaran, Indonesia.

Declaration of Generative AI in Scientific Writing

Generative AI software was utilized solely to edit the readability and words of this manuscript. All was developed under strict human control and oversight, and the authors alone are accountable for accuracy and integrity of the work. No data analysis, interpretation, or scientific content creation was performed utilizing any generative AI software. In compliance with guidelines of authorship, no AI software is listed as authors or contributors.

CRediT Author Statement

E. Julaeha: Conceptualization, methodology, review, supervision, validation, and funding acquisition.

A. K. Herjandi: Resources, investigation, software, writing original draft, data curation, editing and visualization.

J. Al-Anshori: Review and supervision.

References

[1] F Melani and S Sulastri. Analisis perbandingan klasifikasi algoritma CART dengan algoritma C 4.5 pada kasus penderita kanker payudara. *Jurnal Teknokompak* 2023; **17(1)**, 171-183.

[2] T Shien and H Iwata. Adjuvant and neoadjuvant therapy for breast cancer. *Japanese Journal of Clinical Oncology* 2020; **50(3)**, 225-229.

[3] IK Kenyori, MS Alamsyah and CI Nurjanah. Studi *in silico* senyawa bioaktif kuersetin kulit jeruk nipis (*citrus aurantifolia*) sebagai agen antikanker payudara. *Berkala Ilmiah Mahasiswa Farmasi Indonesia* 2022; **9(1)**, 1-10.

[4] AC Gomathi, SRX Rajarathinam, AM Sadiq and S Rajeshkumar. Anticancer activity of silver nanoparticles synthesized using aqueous fruit shell extract of Tamarindus indica on MCF-7 human breast cancer cell line. *Journal of Drug Delivery Science and Technology* 2020; **55**, 101376.

[5] E Julaeha, KS Dewi, M Nurzaman, T Wahyudi, T Herlina and A Hardianto. Chemical compositions and antioxidant activities of Indonesian citrus essential oils and their elucidation using principal component analysis. *Preprints* 2020. https://doi.org/10.20944/preprints202011.0586.v1

[6] V Marcillo-Parra, DS Tupuna-Yerovi, Z Gonzalez and J Ruales. Encapsulation of bioactive compounds from fruit and vegetable by-products for food application - A review. *Trends in Food Science & Technology* 2021; **116**, 11-23.

[7] E Julaeha, S Puspita, DR Eddy, T Wahyudi, M Nurzaman, J Nugraha, T Herlina and JA Anshori. Microencapsulation of lime (*Citrus aurantifolia*) oil for antibacterial finishing of cotton fabric. *RSC Advances* 2021; **11(3)**, 1743-1749.

[8] A Todorovic, L Sturm, A Salevic-Jelic, S Levic, IGO Crnivec, I Prislan, M Skrt, A Bjekovic, NP Ulrih and V Nedovic. Encapsulation of bilberry extract with maltodextrin and gum arabic by

freeze-drying: Formulation, characterisation, and storage Stability. *Processes* 2022; **10**(10), 1991.

[9] X Luo, H Song, J Yang, B Han, Y Feng, Y Leng and Z Chen. Encapsulation of escherichia coli strain nissle 1917 in a chitosan - alginate matrix by combining layer-by-layer assembly with CaCl2 cross-linking for an effective treatment of inflammatory bowel diseases. *Colloids and Surfaces B: Biointerfaces* 2020; **189**, 110818.

[10] NN Indriyani, JA Anshori, N Permadi, S Nurjanah and E Julaeha. Bioactive components and their activities from different parts of *Citrus aurantifolia* (Christm.) swingle for food development. *Foods* 2023; **12(10)**, 2036.

[11] E Julaeha, FE Mulyawan, FM Anwar, AWR Akili, N Permadi, Darwati, D Kurnia and T Herlina. Coumarins from *citrus aurantiifolia* (Christm.) Swingle Peel with Potential Cytotoxic Activity Against MCF-7 breast cancer cell line: *In vitro* and *in silico* studies. *Onco Targets and Therapy* 2025; **18**, 441-452.

[12] E Julaeha, WR Puspita, N Permadi, A Harja, S Nurjanah, T Wahyadi and J Al-Anshori. Optimization of citrus aurantifolia peel extract encapsulation in alginate-gelatin hydrogel microbeads for antibacterial wound dressing applications. *Carbohydrate Polymer Technologies and Applications* 2024; **7**, 100406.

[13] NS Pandiangan, L Pratiwi, DR Eddy, T Wahyudi, AS Mulywan and E Julaeha. Aktivitas anti nyamuk mikrokapsul minyak asiri *Citrus aurantifolia* Terhadap *Aedes aegypti*. *Arena Tekstil* 2021; **36(2)**, 73-82.

[14] DE Gusungi, W Maarisit, H Hariyadi and NO Potalangi. Studi Aktivitas Antioksidan Dan Antikanker Payudara (MCF-7) Ekstrak Etanol Daun Benalu Langsat *Dendrophthoe pentandra*. *The Tropical Journal of Biopharmaceutical* 2020; **2020(1)**, 166-174.

[15] A Lui, J New, J Ogony, S Thomas and J Lewis-Wambi. Everolimus downregulates estrogen receptor and induces autophagy in aromatase inhibitor-resistant breast cancer cells. *BMC Cancer* 2016; **16(1)**, 487.

[16] X Luo, G Wang, Y Wang, M Wang, Z Tan, M Luo, L Zhang, Y Song, Y Jia, H Zhou and C Qing. Gibberellin derivative GA-13315 overcomes multidrug resistance in breast cancer by up-regulating BMP6 expression. *Frontiers in Pharmacology* 2022; **13**, 1059365.

[17] K Bajbouj, J Shafarin, MY Abdalla, IM Ahmad and M Hamad. 2017. Estrogen-induced disruption of intracellular iron metabolism leads to oxidative stress, membrane damage, and cell cycle arrest in MCF-7 cells. *Tumor Biology* 2017; **39(10)**, 101042831772618.

[18] T Huang, L Tang, H Wang, L Lin and J Fu. Carbonic anhydrase 12 gene silencing reverses the sensitivity of paclitaxel in drug-resistant breast cancer cells. *Bioengineered* 2021; **12(2)**, 9806-9818.

[19] MQ Abdullah. Therapeutic potential of tumor suppressors in treating breast cancer. *International Journal of Cancer Studies & Research* 2018; **6(3)**, 235-236.

[20] Z Wang, L Li and Y Wang. Effects of Per2 overexpression on growth inhibition and metastasis, and on MTA1, nm23-H1 and the autophagy-associated PI3K/PKB signaling pathway in nude mice xenograft models of ovarian cancer. *Molecular Medicine Reports* 2016; **13(6)**, 4561-4568.

[21] Z Pan, A Avila and L Gollahon. Paclitaxel induces apoptosis in breast cancer cells through different calcium - regulating mechanisms depending on external calcium conditions. *International Journal of Molecular Sciences* 2014; **15(2)**, 2672-2694.

[22] J Feng, T Wen, Z Li, L Feng, L Zhou, Z Yang, L Xu, S Shi, K Hou, J Shen, X Han and Y Teng. Cross-talk between the ER pathway and the lncRNA MAFG-AS1/miR-339-5p/ CDK2 axis promotes progression of ER+ breast cancer and confers tamoxifen resistance. *Aging* 2020; **12(20)**, 20658-20683.

[23] Z Hu, BL Kagan, EA Ariazi, DS Rosenthal, L Zhang, JV Li, H Huang, C Wu, VC Jordan, AT Riegel and A Wellstein. 2011. Proteomic analysis of pathways involved in estrogen-induced growth and apoptosis of breast cancer cells. *PLoS One* 2011; **6(6)**, e20410.

[24] Y Di, S Cui and Y Gu. Preparation and characterization of a near-infrared light responsive microcapsule system for cancer therapy. *Journal*

of Innovative Optical Health Sciences 2014; **07(01)**, 1350037.

[25] JL Wilson and TC McDevitt. Stem cell microencapsulation for phenotypic control, bioprocessing, and transplantation. *Biotechnology and Bioengineering* 2013; **110(3)**, 667-682.

[26] AH Elmaidomy, UR Abdelmohsen, AM Sayed, FH Altemani, NA Algehainy, D Soost, T Paululat, G Bringmann and EM Mohamed. Antiplasmodial potential of phytochemicals from Citrus aurantifolia peels: A comprehensive *in vitro* and *in silico* study. *BMC Chemistry* 2024; **18(1)**, 60.

[27] N Permadi, M Nurzaman, F Doni and E Julaeha. Elucidation of the composition, antioxidant, and antimicrobial properties of essential oil and extract from *Citrus aurantifolia* (Christm.) Swingle peel. *Saudi Journal of Biological Sciences* 2024; **31(6)**, 103987.

[28] E Sainz, MM Cavenagh, ND LopezJimenez, JC Gutierrez, JF Battey, JK Northup and SL Sullivan. The G-protein coupling properties of the human sweet and amino acid taste receptors. *Developmental Neurobiology* 2007; **67(7)**, 948-959.

[29] Y Ohshima, K Kaira, A Yamaguchi, N Oriuchi, H Tominaga, S Nagamori, Y Kanai, T Yokobori, T Miyazaki, T Asao, Y Tsushima, H Kuwano and NS Ishioka. Efficacy of system: Amino acid transporter 1 inhibition as a therapeutic target in esophageal squamous cell carcinoma. *Cancer Science* 2016; **107(10)**, 1499-1505.

[30] G Ramshankar, R Liu and RJ Perry. The influence of the amino acid transporter lat1 on patient prognosis and the relationships between tumor immunometabolic and proliferative features depend on menopausal status in breast cancer. *PLoS One* 2023; **18(10)**, e0292678

[31] Y Cormerais, M Pagnuzzi-Boncompagni, S Schrotter, S Giuliano, E Tambutte, H Endou, MF Wempe, G Pages, J Pouyssegur and V Picco. Inhibition of the amino-acid transporter LAT1 demonstrates anti-neoplastic activity in medulloblastoma. *Journal of Cellular and Molecular Medicine* 2019; **23(4)**, 2711-2718.

[32] K Kuriyama, T Higuchi, T Yokobori, H Saito, T Yoshida, K Hara, S Suzuki, M Sakai, M Sohda, T Higuchi, Y Tsushima, T Asao, K Kaira, H Kuwano, K Shirabe and H Saeki. Uptake of positron emission tomography tracers reflects the tumor immune status in esophageal squamous cell carcinoma. *Cancer Science* 2020; **111(6)**, 1969-1978.

[33] C Barthelemy and B Andre. Ubiquitylation and endocytosis of the human LAT1/SLC7A5 amino acid transporter. *Scientific Reports* 2019; **9(1)**, 16760.

[34] M Maimaiti, S Sakamoto, Y Yamada, M Sugiura, J Rii, N Takeuchi, Y Imamura, T Furihata, K Ando, K Higuchi, M Xu, T Sazuka, K Nakamura, A Kaneda, Y Kanai, N Kyprianou, Y Ikehara, N Anzai and T Ichikawa. Expression of L-type amino acid transporter 1 as a molecular target for prognostic and therapeutic indicators in bladder carcinoma. *Scientific Reports* 2020; **10(1)**, 1292.

[35] BK Zhang, AM Moran, CG Bailey, JE Rasko, J Holst and Q Wang. EGF-activated PI3K/Akt signalling coordinates leucine uptake by regulating LAT3 expression in prostate cancer. *Cell Communication and Signaling* 2019; **17(1)**, 83.

[36] CM Sevigny, S Sengupta, Z Luo, L Jin, D Pearce and R Clarke. The role of SLC7A5 (LAT1) in endocrine therapy-resistant breast cancer. *Cancer Research* 2019; **79(4S)**, P2-06-14.

[37] M Sato, N Harada-Shoji, T Toyohara, T Soga, M Itoh, M Miyashita, H Tada, M Amari, N Anzai, S Furumoto, T Abe, T Suzuki, T Ishida and H Sasano. 2021. L-type amino acid transporter 1 is associated with chemoresistance in breast cancer via the promotion of amino acid metabolism. *Scientific Reports* 2021; **11(1)**, 589.

[38] OM Ahmed, SF AbouZid, NA Ahmed, MY Zaky and H Liu. An Up-to-date review on citrus flavonoids: Chemistry and benefits in health and diseases. *Current Pharmaceutical Design* 2021; **27(4)**, 513-530.

[39] PHC Campelo, VS Birchal, DA Botrel, GR Marques and SV Borges. Physicochemical and thermal stability of microcapsules of cinnamon essential oil by spray drying: Physicochemical and thermal stability. *Journal of Food Processing and Preservation* 2016; **41(3)**, e12919.

[40] A Parikh and D Madamwar. Partial characterization of extracellular polysaccharides from

cyanobacteria. *Bioresource Technology* 2006; **97(15)**, 1822-1827.

[41] AP Putra, AA Rahmah, N Fitriana, SA Rohim, M Jannah and D Hikmawati. The effect of glutaraldehyde on hydroxyapatite-gelatin composite with addition of alendronate for bone filler application. *Journal of Biomimetics, Biomaterials and Biomedical Engineering* 2018; **37**, 107-116.

[42] AA Abd and Z Al-Khafaji. Gelatin and arabic gum-based food coating for food packaging. *Kufa Journal of Engineering* 2024; **15(3)**, 213-230.

[43] SR Obireddy, C Madhavi, C Kashayi, KRKS Venkata and SMC Subbarao. Gelatin-coated dual cross-linked sodium alginate/magnetite nanoparticle microbeads for controlled release of doxorubicin. *ChemistrySelect* 2020; **5(33)**, 10276-10284.

[44] S Caglar and DA Sahbaz. Ultrasonic-assisted synthesis, characterization, and release kinetics of Sweetgum (*Liquidambar orientalis* Miller) essential oil microcapsules as efficient antibacterial materials. *Research Square* 2023; **1**, 1-20.

[45] SR Derkach, NG Voron'ko, YA Kuchina and DS Kolotova. Modified fish gelatin as an alternative to mammalian gelatin in modern food technologies. *Polymers* 2020; **12(12)**, 3051.

[46] F Menichini, MR Loizzo, M Bonesi, F Conforti, DD Luca, GA Statti, BD Cindio, F Menichini and R Tundis. Phytochemical profile, antioxidant, anti-inflammatory and hypoglycemic potential of hydroalcoholic extracts from Citrus medica L. cv Diamante flowers, leaves and fruits at two maturity stages. *Food and Chemical Toxicology* 2011; **49(7)**, 1549-1555.

[47] A Maugeri, A Calderaro, GT Patane, M Navarra, D Barreca, S Cirmi and MR Felice. Targets involved in the anti-cancer activity of quercetin in breast, colorectal and liver neoplasms. *International Journal of Molecular Sciences* 2023; **24(3)**, 2952.

[48] J Martinovic, R Ambrus, M Planinic, G Selo, A Klaric, G Perkovic and A Bucic-Kojic. Microencapsulation of grape pomace extracts with alginate-based coatings by freeze-drying: Release kinetics and *in vitro* bioaccessibility assessment of phenolic compounds. *Gels* 2024; **10(6)**, 353.

[49] NDA Aceval, PMD Medeiros, ES Prudencio, CMO Muller and RDDMC Amboni. Encapsulation of aqueous leaf extract of Stevia rebaudiana Bertoni with sodium alginate and its impact on phenolic content. *Food Bioscience* 2016; **13**, 32-40.

[50] SAA Murtadza, NAM Zaki, J Jai, F Hamzah, NS Ashaari, DS Fardhyanti, Megawati and NAC Imani. 2024. Microencapsulation of citrus hystrix essential oil by gelatin B/Chitosan complex coacervation technique. *Pertanika Journal of Science and Technology* 2024; **32(2)**, 599-621.

Supplementary Material

Table S1 Structures of ligands and their interactions with receptors on 3ERT, 3PY0, and 1KV1 proteins.

No.	Ligand structure	Interaction with receptor's amino acid binding pocket
1	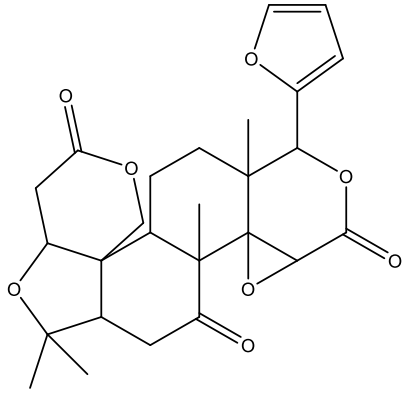 Evodin (3) with 3ERT receptors	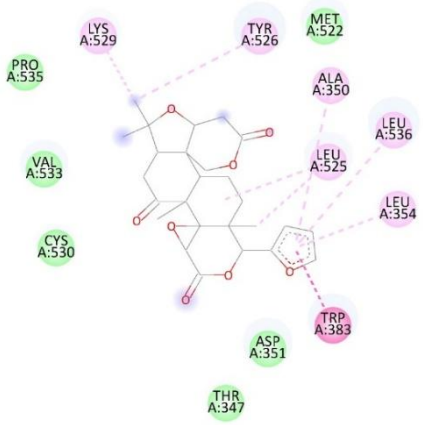
2	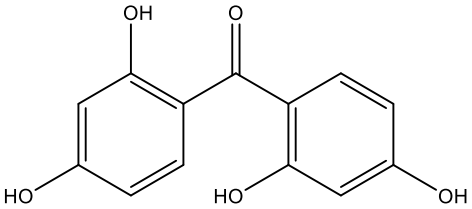 2,4,4′,6′-Tetrahydroxybenzophenone (2) with 3PY0 receptors	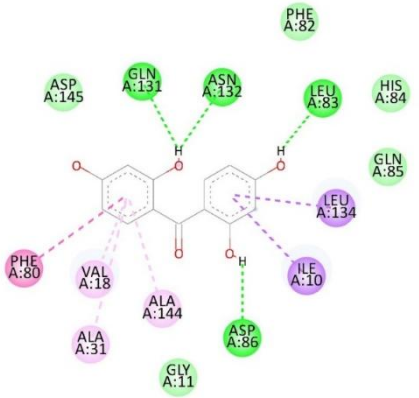
3	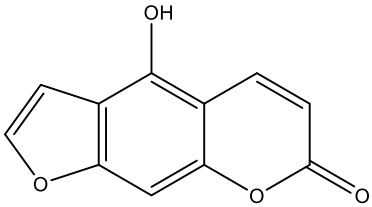 Bergaptol (4) with 3PY0 receptors	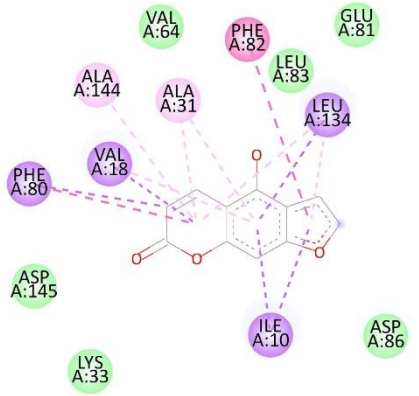

No.	Ligand structure	Interaction with receptor's amino acid binding pocket
4	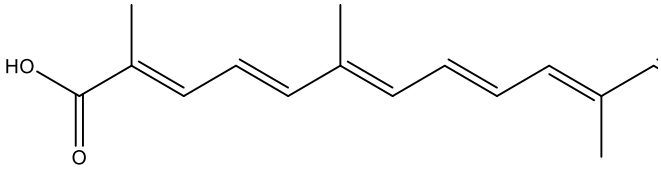 Crocetin (5) with 3PY0 receptors	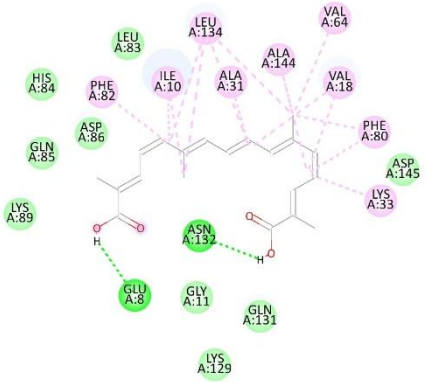
5	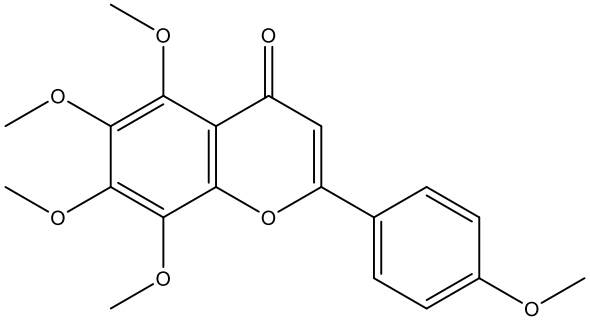 Tangeretin (7) with 3PY0 receptors	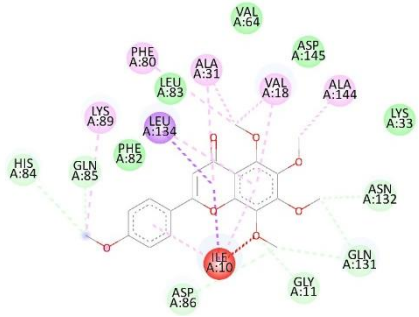
6	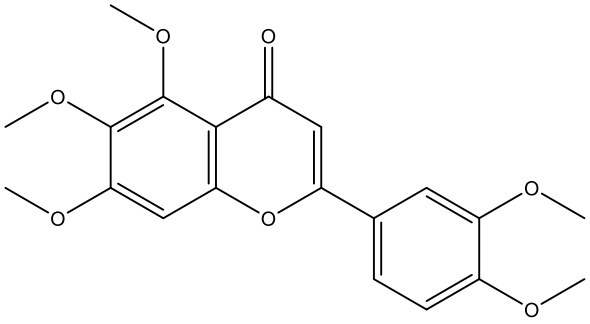 Sinensetin (9) with 3PY0 receptors	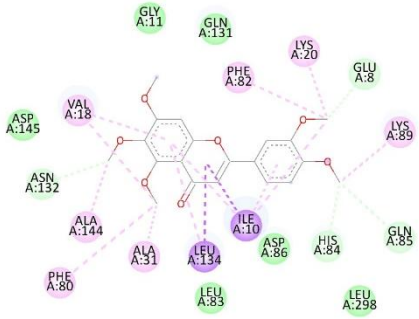
7	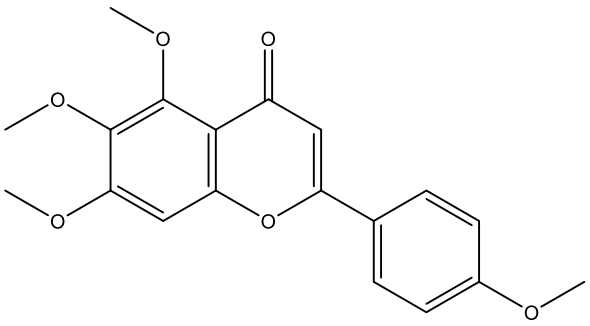 Tetramethylscutellarein (10) with 3PY0 receptors	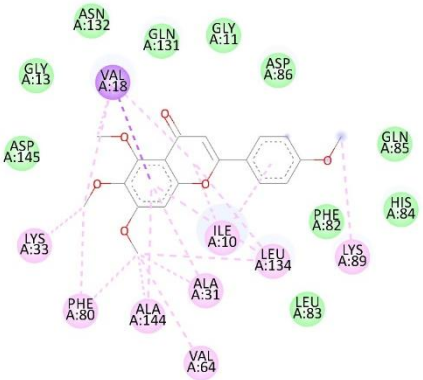

No.	Ligand structure	Interaction with receptor's amino acid binding pocket
8	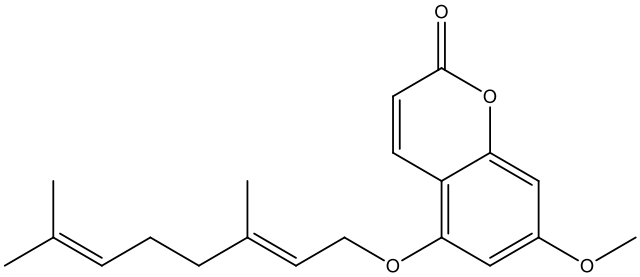 5-Geranyloxy-7-methoxy coumarin (11) with 3PY0 receptors	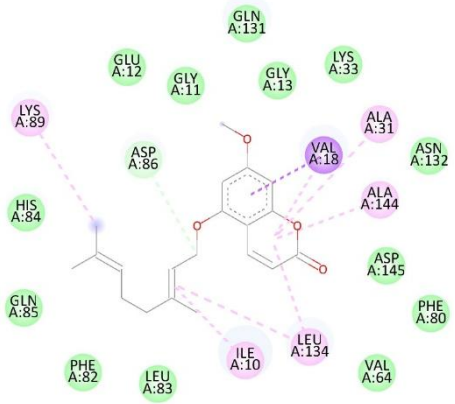
9	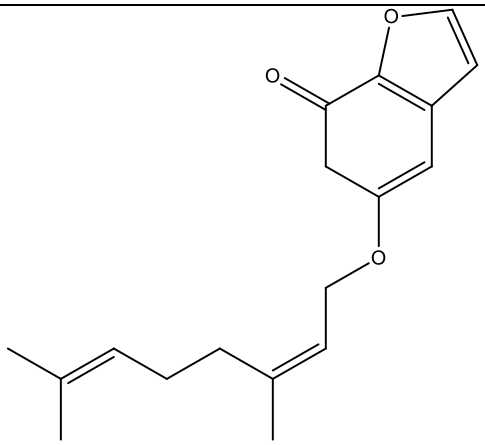 5-Geranyloxypsoralen (12) with 3PY0 receptors	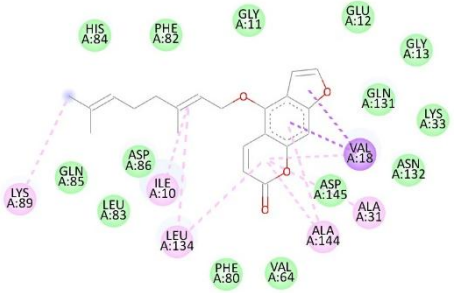
10	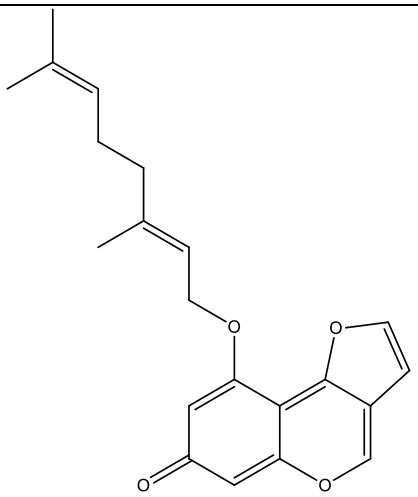 8-Geranyloxypsoralen (13) with 3PY0 receptors	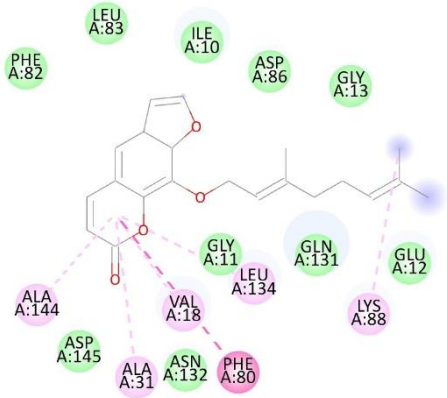

No.	Ligand structure	Interaction with receptor's amino acid binding pocket
11	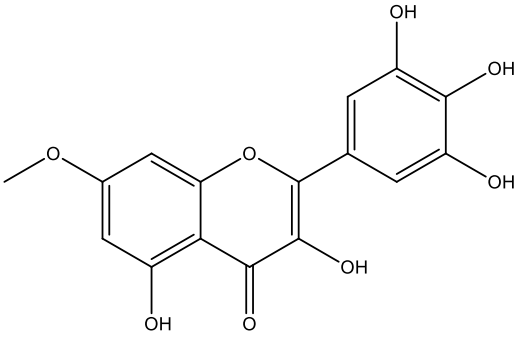 Europetin (15) with 3PY0 receptors	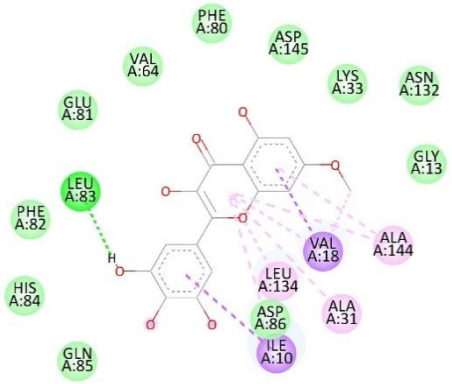
12	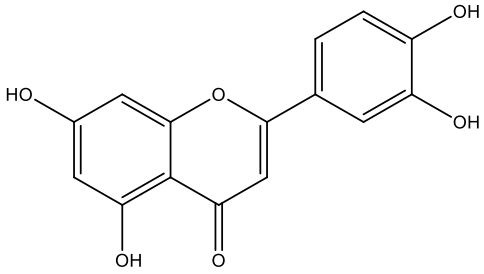 Luteolin (16) with 3PY0 receptors	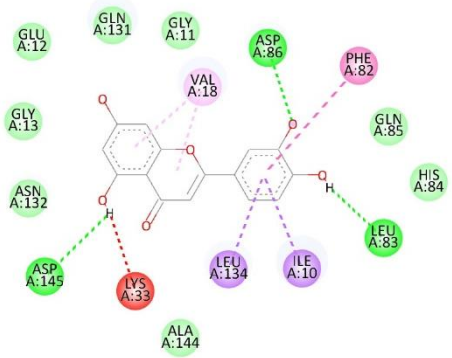
13	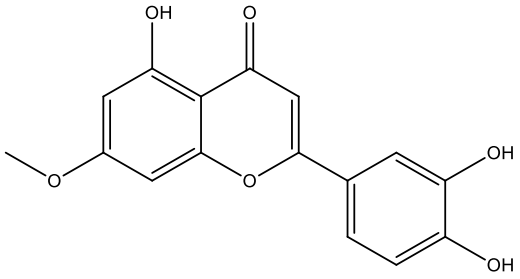 3`-Hydroxygenkwanin (18) with 3PY0 receptors	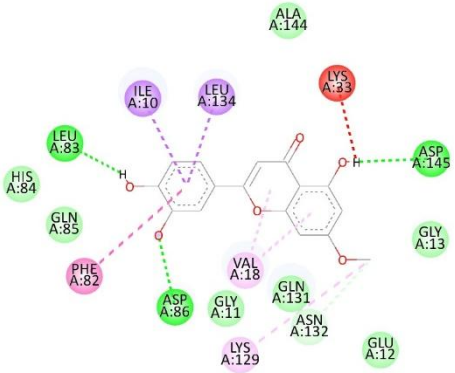
14	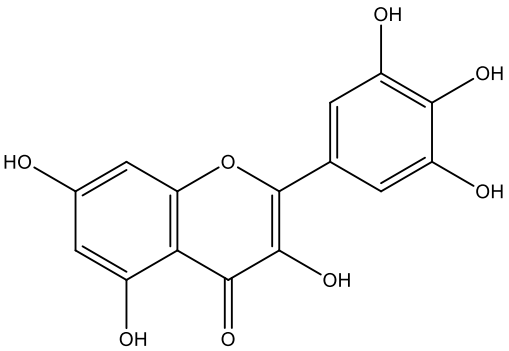 Myricetin (19) with 3PY0 receptors	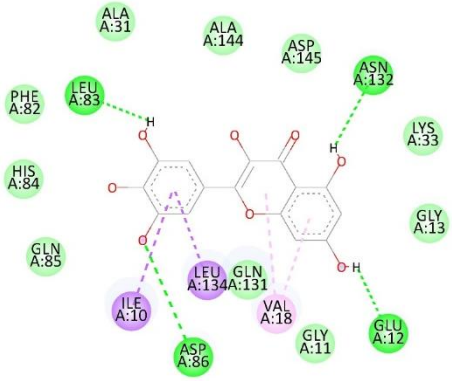

No.	Ligand structure	Interaction with receptor's amino acid binding pocket
15	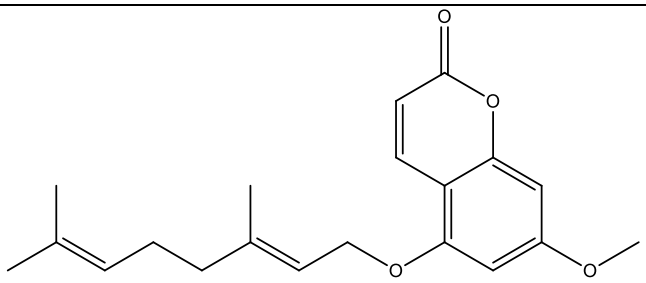	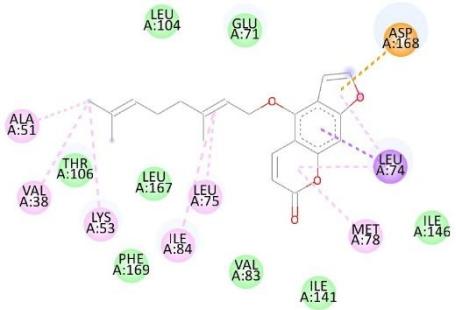
	5-Geranyloxy-7-methoxy coumarin (11) with 1KV1 receptors	
16	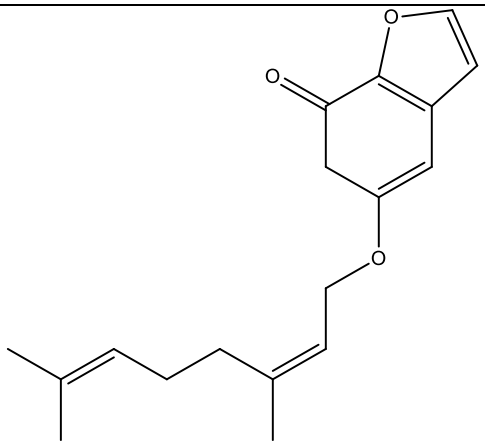	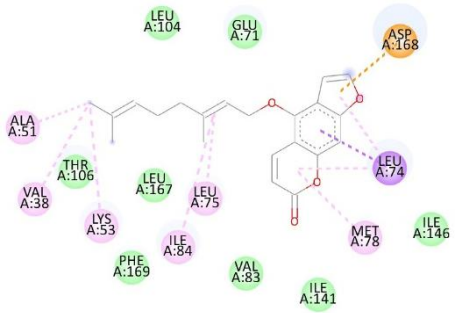
	5-Geranyloxypsoralen (12) with 1KV1 receptors	

*notes: